# Multiscale modeling for
# photoinduced processes in composite systems

Benedetta Mennucci[1*] and Stefano Corni[2*]

**Abstract** | In the last decades, the quantum mechanical modeling has moved from isolated molecules made of few atoms, to large supramolecular aggregates embedded in complex environments. This has been made possible by the important progress achieved by multiscale models based on the integration of QM methods with classical descriptions. One of the first example of this integration is represented by continuum solvation models that starting from the eighties of the last century have been largely and successfully applied to predict properties and processes of solvated molecules. Almost in the same years, another alternative classical description, based on Molecular Mechanics (MM) has been coupled to QM methods to give the hybrid QM/MM approach. Since their first formulations, these QM/classical models have seen an enormous development in terms of accuracy, robustness and generalizability. This progress has allowed their application to systems of increasing complexity and to processes never faced before within a QM framework. An important example of such an achievement is represented by the novel insights reached in the fundamental understanding and the possible exploitation of photoinduced processes in biomolecules, nanomaterials and, more in general, composite systems where different "objects" of molecular, nano and mesoscopic scale are coupled together. In this review, we highlight the potentials and the limitations of such modeling, thereby showing which developments are still needed to definitely make the QM-based multiscale strategy the gold-standard for explaining the outputs of novel advanced spectroscopic techniques and predicting the outcome of light-activated events in composite systems.

[1] Department of Chemistry, University of Pisa, v. Moruzzi 13, 56124 Pisa, Italy. Email: benedetta.mennucci@unipi.it
[2] Department of Chemical Sciences, University of Padova, v. Marzolo 1, 35131 Padova, Italy, Email: stefano.corni@unipd.it

The response of molecules to light represents one the most effective ways to investigate their properties through the vast set of spectroscopic techniques which are based on the detection and quantification of such a response. As a matter of fact, light is also used by "special" (supra)molecular systems to activate processes spanning many time and space scales. To achieve such a multiscale character, these systems are generally composite, i.e. they contain recognizable constituents with different characteristics in terms of chemical composition, size and behavior. Nature has often used these photoresponsive composite systems as a very effective tool to perform a specific biological function. Inspired by such an incredible strategy, scientists have started to design artificial composite systems which, using light, can achieve enhanced or completely new properties with respect to the single components.[1-4] However, the rational of the photo-induced processes in both natural and artificial composite systems is still far from being complete. It is therefore extremely important to develop tools which can be used to explain the natural processes and to conceive artificial setups which not only mimic the former but also optimize them according to our requirements. These tools need to combine a good theoretical foundation with an efficient computational machinery able to simulate systems going well beyond the molecular scale. This is clearly a challenging task.

If the photoinduced process can be localized on a specific part of the system, its effective modeling can be achieved introducing a "focused approach". Here, the term "focused" is used instead of the more general one, "multiscale", to recall that we are considering embedded systems, where a finite subsystem is surrounded by a larger (and eventually infinite) *environment*. These are clearly a subfamily of the vast world of multiscale systems, and in particular they do not contain the important case of (nano)materials, for which the multiscale modeling has been largely used but it will not be reviewed here. [5-7]

Within this focused formulation of multiscale approaches, the subsystem of interest (from now on the "*target*") is represented as a set of interacting quantum mechanical (QM) units (atoms, molecular fragments, up to molecular aggregates), which are embedded in a "classical" *environment* acting back on the target. To account for that, the environment itself does not need to be described at atomic or molecular level; what is here important is in fact the "action" of the environment on the target. In a QM language, this means that we have only to define the operator(s) to be added to the QM Hamiltonian of the target to account for such an action. If this operator can be correctly formulated even without knowing the atomistic nature of the environment, the goal will be anyhow achieved as the focus is in the embedding effects on the target and not on the accurate description of the whole system (target+environment).

This simple statement of course hides many fundamental details which make the operative formulation of the focused approach nor univocal neither simple.

The main issues are (i) the definition of the target (and the boundary between the target and the environment), (ii) the nature of the action of the environment on the target and (iii) the role of reciprocity in such an action.

Obviously, the definition of the target determines the type of action of the environment. In fact, by enlarging the subsystem which defines the target so to include the atoms/molecules of the environment which strongly interact with it, the action of what remains of the environment can be described through long-range (mostly) electrostatic effects. If, instead, the target is limited to the molecular system of interest, the action should go beyond electrostatic and include short-range repulsion and dispersion effects as well. The beauty of this approach is exactly that: in the limit of the computational feasibility and with the constraint that no charge-transfers are possible between the target and the environment, any choice of the boundary is possible, and the description can be systematically improved on the basis of the system and the process of interest.

The issue of the reciprocity is also strictly connected to the definition of the target but, this time, the improvement of the description is not as straightforward as before because mutual effects between the target and the environment enter into play.

**The multiscale strategies**

In the years, two main strategies to combine QM descriptions of the target and classical models of the environment, have been proposed. Interestingly, their first formulations date back to the same years, namely the end of the seventies of the previous century. [8-10]

The two strategies refer to continuum and discrete (or atomistic) descriptions of the environment, respectively. In the latter case, the atoms of the environment (or group of atoms in coarser grained versions of the model) are treated through a Molecular Mechanics (MM) force field (FF). [11-15] In the former case, instead, the atomic nature of the environment is lost and a continuum description in terms of macroscopic properties is introduced instead. [16-18]

Despite this huge "modellistic" difference, the two formulations present important common elements when reconsidered from the point of view of the QM target. In any case, for simplicity's sake two separate presentations will be given.

*QM/continuum.* If the environment loses its atomic nature, an effective description has to be introduced which is based on some macroscopic properties. This is exactly what is done in continuum models where the target sees the environment as an infinite dielectric medium characterized by a (generally) frequency and position dependent permittivity tensor function $\varepsilon(\omega;r)$. In the most common formulations of the model, however, a homogeneous and isotropic approximation of the dielectric medium is introduced, and the permittivity function loses its position dependency and becomes a scalar quantity. Moreover, for standard applications of the model also the frequency dependency can be neglected, and a single value is used, namely the isotropic dielectric constant of the environment of interest, $\varepsilon$. As a matter of fact, the position and frequency dependence will be reintroduced later when extensions of the model to heterogeneous environments and dynamic processes will be presented. The dielectric constant is a measure of the response of the medium to an applied electric field and is an experimentally known property for most of the common solvents: on the basis of its value, solvents are classified as apolar (i.e. non-responsive to electric fields such as cyclohexane where $\varepsilon\sim2$) or polar (i.e. highly responsive such as water where $\varepsilon\sim80$).

Together with the value of the dielectric constant of the environment, the continuum models require to define the boundary of the target, which, in this context, is called "cavity surface". The target is in fact assumed to be fully contained within a cavity which, in its most accurate formulation, should follow the geometrical structure of the target itself. In the old versions of continuum models, simplified cavities have been largely used, such as spheres and ellipses, because in those cases an analytical solution of the electrostatic problem is possible. In all the other cases instead, a numerical solution has to be introduced.

Many different numerical strategies have been proposed so far but within the quantum chemical formulation of the model, the one which has shown to be the best compromise between accuracy, generality and computational feasibility is the so-called *Apparent Surface Charge* (ASC) approach (see Box 1). [19-21] Different cavities have been used in combination with the ASC formulation; in most cases, a set of interlocking spheres centered on the target atoms is used with radii defined so to take into account the atomic dimension but also the dimension of the solvent molecules (the resulting cavity surface is also known as Solvent Accessible Surface, SAS).

Within the ASC formulation, the main idea is that the action of the environment on the target can be described in terms of a set of "apparent" charges placed on the cavity surface only. These surface charges are "apparent" as they exist only if a source of polarization exists, here the QM charge density of the target. The number of ASCs is determined by the cavity and the mesh used for partitioning its surface while their values depend on the dielectric constant of the environment and the QM density of the target. Because of the dependence of the ASCs on the QM density, and of the latter on the action of the ASCs, a self-consistent approach is needed; the name "*self consistent reaction field*" (SCRF) is also

commonly used to identify this approach when combined with a SCF QM method such as Hartree-Fock (HF) or Density Functional Theory (DFT).

From this brief description, it is evident that the ASC formulation of continuum models automatically accounts for the mutual polarization between the target and the environment (see Fig. 1).

In the years, the ASC models have been reformulated many times and nowadays they represent extremely robust and efficient numerical methods. Moreover, they have been extended to almost all the applications of quantum chemistry for isolated molecules such as the study of the potential energy surfaces, the simulation of chemical reactivity and the prediction of spectroscopic properties. This has been made possible thanks to the simplicity of the ACS formulation which introduces an additional operator to the Hamiltonian of the isolated system which is very easy to calculate and to be analytically differentiated with respect to external and internal perturbations (geometrical distortions, external electric and magnetic fields, etc.). The latter characteristic in particular has allowed to combine continuum models with response theories, thus achieving a computationally effective and general approach to include environment effects in the simulation of spectroscopies.

As a matter of fact, the extension of continuum models to light-matter interaction is not automatic but it requires to face two important aspects which are not present when the same phenomenon is simulated for an isolated system. When an oscillating field impinges on an embedded system, the time-dependent reaction of the latter will be necessarily coupled to that of the environment. Normally, the environment should be transparent with respect to the applied field. If this is the case, the applied field oscillates at frequencies that are far from possible resonances of the molecules of the environment, and, in our modeling, we can avoid to explicitly consider the environment frequency dependent response. However, we cannot completely neglect the timescale of such a response with respect to that of the target. In fact, if the dynamics of the process induced in the target by the oscillating field is faster than the response in the environment, the latter will (fully or partially) lag behind. This is what happens when we consider an electronic transition in the target: the system which is initially in equilibrium with the environment, instantaneously is excited to a new electronic state corresponding to a new electronic density while the environment is still in the original configuration. The delay in the environment response will correspond to a kind of *nonequilibrium* which will eventually relax to a new equilibrium once the environment configuration will be optimally adapted to the new electronic density in the target. This relaxation will be possible if the lifetime of the excited state is long enough with respect to the time scale of the environment relaxation. In common polar solvents, the timescales involved in the solvation dynamics are of the order of some hundreds of ps, e.g. much slower than a vertical excitation but faster than molecular excited state lifetimes. This means that the emission following the excitation will happen with a solvent which has been fully equilibrated to the excited target and the whole nonequilibrium scheme should be reverted.

When these molecular responses of the environment are "translated" into a macroscopic language we can distinguish between optical and static dielectric constants. The optical one describes the fast response of the dielectric to fields of very high frequency (high with respect to the excitation frequencies of the solute) and can be approximated with the square of the refractive index at optical frequencies, while the static one is the "total" response to static fields: just to quantify the two relative values, for the most common polar solvent (water) we have $\varepsilon_{opt}=1.7$ and $\varepsilon_0=78$.

This simplified picture is extremely effective when integrated into the framework of ASC models. In fact, we can assume that also the apparent charges can be split into two components: a dynamic one corresponding to the electronic degrees of freedom of the environment molecules and an inertial one corresponding to their nuclear and orientational motions. In our effective model, an electronic excitation in the target will induce a change only in the dynamic charges (determined by $\varepsilon_{opt}$) while the rest will remain frozen. In practice, this means that all environments behave as apolar ones during the electronic transition.

4

Even when the interaction with applied field does not induce an excitation in the target system, still the presence of the environment makes the process different from the case of an isolated system. The applied field in fact will polarize the environment and as a result the field acting at the molecular level on the target will be different from the applied one. This effect is well known since many years and it is generally described as *cavity field effect*. Its main application is within nonlinear optics to properly connect measurements of electric response properties (electric susceptibilities) of chromophores dispersed in a macroscopic condensed medium to the corresponding molecular polarizabilities. The common approach is to use the simple correction factor proposed by Lorentz and by Onsager[22] based on simplified continuum models. Important generalizations of the Onsager-Lorentz model have been made in the years by using more refined ASC approaches. [23] Within this context, the field acting locally on the target is described through an additional set of apparent charges induced on the cavity surface not by the molecule itself but by the externally applied field. In general, such new set of charges depends not only on the solvent macroscopic properties but also on the details of the molecular cavity and, when the cavity is very far from a simple sphere, the description of the cavity field effects can be significantly different from the standard Lorentz or Onsager factors. These effects are quite general, as all properties depending on an external field need to account for them; this is true, for example, for Infrared and Raman intensities, but also for absorption and emission intensities.

A particularly intriguing kind of light-matter interaction in the presence of an active environment is that comprising a (solvated) molecule in proximity of a metallic nanostructure. Here, the incoming light is also able to excite a surface plasmon (a collective excitation of the metal conduction electrons), that in turn can greatly amplify the electric field locally. There are several phenomena where this is used. In spectroscopy, nanoparticles, metal surfaces with nanoscale roughness or tip with nanoscale radius of curvature are exploited to enhance the signal from the molecule. [24] The best-known example is undoubtedly Surface Enhanced Raman Spectroscopy (SERS or TERS in the metallic tip-enhanced version)[25,26] where the Raman scattering signal of molecules are enhanced by several order of magnitude.[27] Single molecule and even sub-single molecule (i.e., intramolecular) resolution has been demonstrated.[28,29] Plasmonic effects have become largely used for sensing applications (e.g. through SERS but also plasmon-enhanced fluorescence[30,31] and other techniques).[32,33] In photochemistry, plasmonic nanostructures are used to promote photoreactions,[34-36] either by exploiting the enhanced excitation due to plasmons or by transfer to the molecule hot carriers which have been generated inside the metal by the light. In another class of experiments, the molecule-nanostructure interaction can be so strong to reach the level where hybrid light-molecule states are in order to describe the system (strong coupling regime).[37,38]

In the electromagnetic mechanisms of these phenomena[39] there is a close analogy with what already discussed for molecules in solution. The external field enhanced by the plasmonic resonance is what is called cavity field for molecules in solution; the field acting on the molecule and due to the nanoparticle polarization induced by the molecule itself (sometimes called image field) is the analogous of the reaction field in solution. The effects of such fields are much more dramatic in the case of metal nanostructures due to the plasmonic excitation, but the formal analogy is very strict. An important difference between molecules close to metal nanoparticles and in solution lies in the much more relevant role of metal-molecule charge transfer, that is a (quantitatively minor) contribution to SERS but is the central effect in hot-carrier induced photochemistry. Many phenomena however can be captured by purely electromagnetic models, as it has been shown in the literature.

Once the analogy with molecules in solution has been made explicit, it is not surprising that the multiscale models developed so far for molecules close to metal nanoparticles bear a strong resemblance with those developed for molecules in solution. Also in this case, scientists put forward multiscale models that describe the metal as a continuous dielectric medium, and others that exploit an atomistic description of the metal.[40] The older of the continuum models for molecule-plasmon systems is based

on the ASC description described above (see also Box 1).[41] Seen from the point of view of the classical electromagnetic models for plasmonics, the metal nanoparticle is treated with a quasistatic version of the Boundary Element Method (BEM) approach (fully retarded BEM are also extensively used in nanoplasmonics).[42,43] It is worth remarking that the continuum description of a solid nanoparticle has not been limited to metal, but was suggested for semiconductor NP as well, exploiting a similar philosophy.[44] The use of continuum models for molecules interacting with metal specimen has also been proposed as a convenient approach in photoelectron spectroscopy. [45] Finally, intermediate descriptions where the molecule and the metal specimen are not mutually coupled, but rather the local electromagnetic field is calculated a priori without the molecule and then applied on the molecule, approximately taking into account its spatial dependence, have been also proposed and proved to be useful. [46]

A recent turn in the development of such models is the transition to approaches that describe the interaction with light in the *time domain* rather than in the frequency domain. On one hand, this allows to simulate directly experiments where light pulses, often of complicated profiles, are involved. [47] It also allows to include naturally important effects such as decoherence and relaxation. On the other hand, it may have computational advantages, related to the different scaling of the computational cost with the system size of the time-dependent vs frequency calculations (many matrix-vector multiplications in one case vs a single iterative matrix diagonalization in the other). [48] In practice, the time-dependent approach amounts to numerically solve a time-dependent Schrödinger equation for the molecule (or its DFT counterpart, i.e., a time-dependent Kohn-Sham equation) electromagnetically coupled to a numerical time-dependent classical electromagnetic solver.[49,50] The Finite Difference Time Domain solver coupled to real-time TDDFT is the most natural choice.[51-54] A time-dependent formulation of the ASC approach is also possible and may have technical advantages in the calculation of the electromagnetic coupling. [55]

*QM/MM.* The continuum approach presented so far is an extremely flexible and effective approach to include environment effects within a focused formulation. In particular, the use of the ASC formulation of continuum models based on molecular cavities which accurately follow the chemical and structural composition of the target has largely improved the sensitivity of continuum models to "local" effects due to the presence of specific chemical groups in the target which can differently interact with the environment. These effects were completely neglected in older formulations of continuum models based on very simplified cavities (often a single sphere) and assuming a monopolar or dipolar distribution of charge for the target.

However, it is clear that continuum models cannot be the solution of all problems. The lack of the atomic nature of the environment necessarily excludes the chance of a correct and accurate description of any specific interaction between the target and the environment. Moreover, molecular-scale heterogeneities/anisotropies in the environment are lost as well when using a continuum model.

In all cases where these specificities play a significant role, the alternative atomistic strategy for the environment has to be preferred. As reported in the Introduction, the coupling of atomistic or continuum classical models with QM descriptions has been proposed in the same years. Because of that, both strategies have a long history behind, and many fundamental improvements have been proposed during the years both from the numerical and the modeling point of view. When talking about atomistic formulations, the standard approach is to introduce a MM Force Field to describe the atoms of the environment. As a result, the QM target will be coupled through electrostatics and through dispersion-repulsion potentials. As a matter of fact, also covalent bonds between the target and the environment are possible within this framework, and they are generally addressed by introducing some "tricks" such as the link atoms or the frozen density approaches. Going back to noncovalent interactions, the most common formulation of QM/MM limits the action of the MM part on the QM target to electrostatics,

only recovering the dispersion and repulsion terms as additional fully classical energy corrections. This is exactly the common "*electrostatic embedding*" version of QM/MM methods where the QM density "sees" the environment as a set of fixed point-charges (or a fixed multipolar expansion) representing the MM atoms.

Especially in the last years, this formulation has been often supplemented with the inclusion of an additional term accounting for the polarization of the environment. The resulting "*polarizable embedding*" has been realized in many different ways.[56] One way is to replace the fixed charges of the electrostatic embedding with fluctuating ones which are defined through the electronegativity equalization. [57-61] Another strategy is to introduce a Drude oscillator model where a charge is located at the MM atom, while a second charge of the same magnitude and opposite sign is mobile.[62,63] The two charges are linked by a harmonic spring and, as a result, the polarization arises from the competition between the forces acting on the mobile charge, which are due to the spring and the electrostatic interactions with the environment. A third approach is the one based on induced dipoles.[64-68] Here, each MM atom is characterized by a fixed charge and a (usually isotropic) polarizability: as a result of the electric field due to the target (and the MM charges) an induced dipole will appear on each atom of the environment.

In all cases, mutual polarization effects between the target and the environment will be included exactly as done in the continuum framework but this time also keeping the atomistic details of the environment. As a matter of fact, by moving from the electrostatic to the polarizable (pol) embedding, the QM/MM and the continuum formulations become more and more similar. For example, also for the QM/MM(pol) we can introduce the SCRF concept where the target density and the polarization of the environment are solved together exploiting a variational formulation. Moreover, the QM/MM(pol) can properly take into account possible nonequilibrium effects through the separation between an inertial (the fixed charges) and a dynamic (the induced dipoles) component of the MM description.[67,69,70] Only the dynamic part will be able to respond to an instantaneous change in the charge distribution of the target while the inertial component will remain frozen in its initial configuration, i.e. the induced dipoles will change in value but their position as well as the fixed charges will remain "frozen". Finally, also the cavity field effect can be described through QM/MM(pol) by using additional induced dipoles to simulate the change of an externally applied field at the target.[71,72]

All these evident similarities between continuum and MM(pol) descriptions of the environment however should not generate the erroneous idea that the two approaches are, in some way, interchangeable. Indeed, the two methods require a completely different application strategy (see figure 1). While the continuum model does not require any knowledge about the spatial distribution of the environment atoms, the MM does. This has two important consequences: the first one is that any QM/MM calculation has to be preceded by the determination of the atomic positions of all the MM atoms. The second is that one single calculation referring to one MM configuration is often not enough, and many different configurations have to be used to get a correct sampling of the environment, paying particular attention to avoid getting stuck in a subset of local free energy minima (e.g., specific conformations of the QM portion or of the complex MM environment).

This sampling is indeed mimicking a realistic feature of the system, but it also represents a strong practical limitation of QM/MM approaches as it involves a much larger computational cost with respect to the continuum analog. Commonly, QM/MM calculations are combined to fully MM molecular dynamics (MD) simulations which are used to get the various configurations of the system. This is a cost-effective approach, but it can suffer an important weakness: the common FFs are not always accurate enough to give proper geometries of the chromophoric units to be directly used in the following QM description of the target.[73,74] Different possible strategies have been proposed in the literature to solve this problem. The first one is to define optimized FFs for chromophores by parameterizing them on the basis of QM calculations.[75] An alternative strategy is, instead, to introduce "ab initio" (or QM) FFs which are fully built on first principles and require no fitted parameters.[76] Very

popular examples of this type are the Effective Fragment Potential (EFP) method[77] and the X-Pol strategy.[78] A third solution is to use a QM/MM molecular dynamics.[14] Of course, the much larger cost of this approach has so far limited its applications but recently more efficient implementations have been made available[79,80] also within a polarizable embedding. [81]
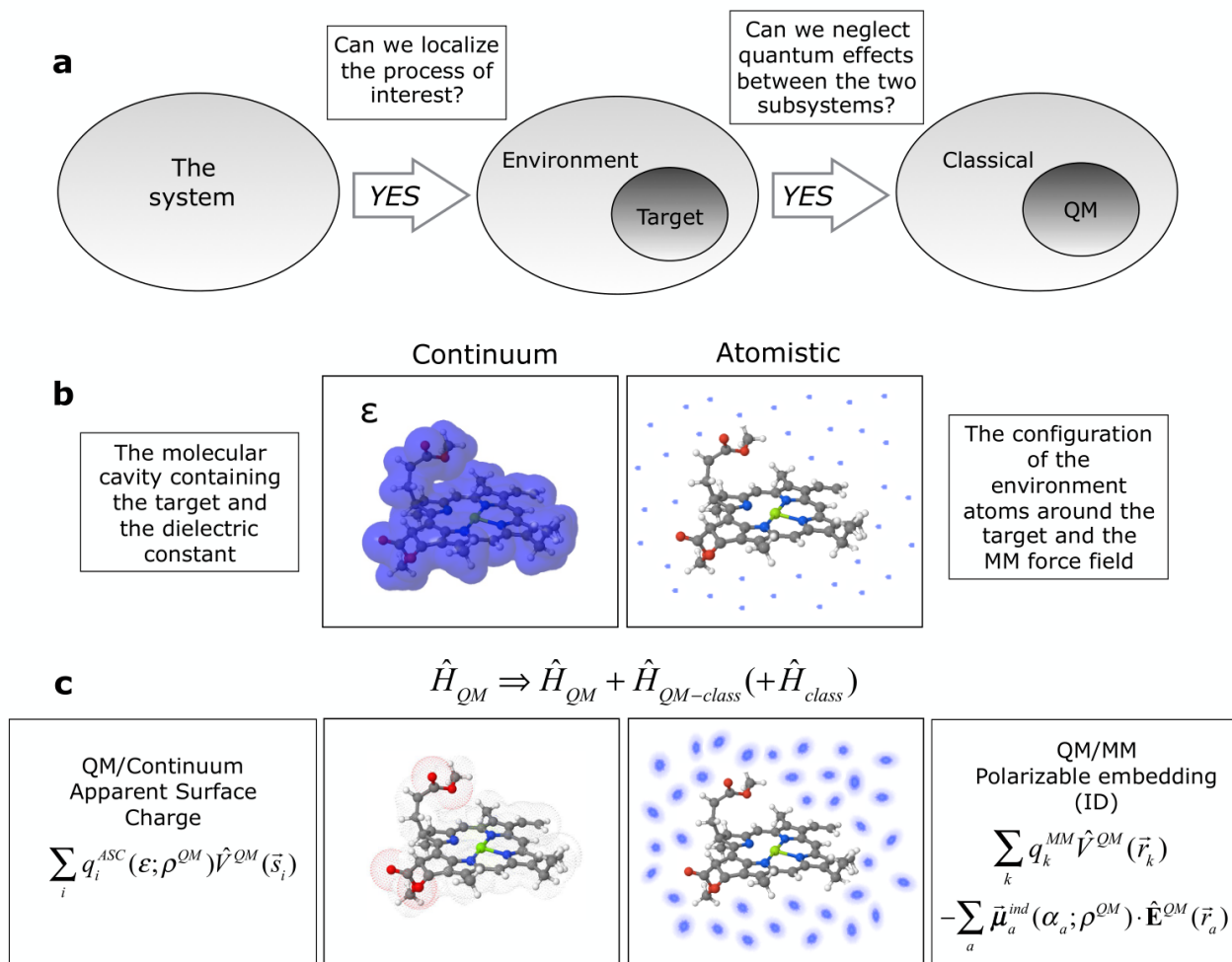


**Figure 1. The QM/classical strategy**. a) The conceptual way which leads to the selection of a hybrid QM/classical approach. b) The input data needed in the continuum and the atomistic formulation of the classical environment. c) The effective Hamiltonian within two popular formulations of continuum and MM models: the former refers to the ASC approach and the latter to the ID type of polarizable embedding (the purely classical term applies only for the MM formulation).

Keeping the parallelism with solvation model, the problem of a molecule close to a metallic nanoparticle has been also tackled with a classical but atomistic description of the metal specimen. This approach has been pioneered by Jensen's group, who developed the Discrete Interaction Model (DIM).[82] While for non metallic environments using an electrostatic but unpolarizable embedding is meaningful, this would be of limited use to describe phenomena when plasmonic excitations are involved. For this reason, DIM has been from the very beginning a polarizable embedding approach; this was achieved by allowing for a scalar dipolar polarizability plus a fluctuating charge per each atom, even if, in the most recent version of the model, only the polarizability features are typically exploited.[83] In addition, while atomistic polarizable models for solutions or biomolecular environments adopt a frequency independent polarizability, in DIM the atomic polarizability and the chemical hardness (or rather atomic capacity in the plasmonic context) are frequency dependent (see Box 4). Various prescriptions

have been given to set the metal atom parameters of this model, that in the most recent version depend also on the coordination environment of the metal atom. Similar models have been also incorporated in other descriptions, such as the capacitance-polarization model proposed by Rinkievicius et al. [84]. Moreover, proper metal-solvent-molecule force fields are being developed to include a proper sampling of the ground state geometries.[85]

**The multiscale modeling of photoinduced processes**
In the years, multiscale approaches have been largely applied to study photoinduced processes.[14,86] While in the past decades, the focus was mostly on the simulation of solvatochromism of common solvated dyes, in the last years the attention has been moved to much more complex systems and to excited state processes going beyond the vertical absorption. Here we primarily focus on some of these recent applications while for the examples describing the first phase of the extension of the multiscale methods (either in their continuum and atomistic formulation) to photoinduced processes we refer the reader to earlier reviews.[13,18,87,88]

**Molecules close to surfaces & nanostructures**. It is widely recognized that MNPs generally enhance the radiative decay rates of fluorophores as well as the initial process of electronic absorption.[89,90] However, the presence of metal NPs also activates a new nonradiative channel of decay through excitation energy transfer (EET) from the fluorophore to the NPs, explaining the sometimes very strong fluorescence quenching observed experimentally.[90] Therefore, a global enhancement of a fluorescent system is the result of a competition between local enhancement and quenching. It is also well known that the plasmonic properties determining the final enhancement or quenching of the fluorescence depend not only on the characteristics of the MNP (its nature, shape, and dimension) but also on the position and orientation of the fluorophore with respect to the MNP as well as on the interparticle distance if a multi-MNP system is used. In addition, as the whole process is conducted in solution, the presence of the solvent can significantly affect fluorophore's structure and properties and the NP plasmonic behaviours. It is clear that all these couplings among the different components of the whole system (the fluorophore, the NPs, and the solvent) make the accurate modelling of the process extremely difficult. Within the PCM-NP framework, all these parameters can be included in a single and coherent theoretical approach. Using such an approach, the global effect of the composite environment on the fluorescence of a given molecular system can be determined by calculating the so-called relative brightness ($\Phi^{RB}$). The relative brightness is the quantity more directly related to experiments as it quantifies metal-induced enhancement or quenching of the fluorescence at a constant excitation intensity. It can be computed as the product of a factor which takes into account the different population in the fluorophore excited state induced by the metal influence on the molecular absorption and the fluorescence quantum yield. All the involved quantities (the absorption factor, the radiative, and the nonradiative decay rates which define the quantum yield) can be obtained using the QM/PCM-NP approach which explicitly includes mutual polarization effects among all the components (fluorophore and NPs, fluorophore and solvent, NPs and solvent, and NPs among themselves when an array is considered).
In Fig. 2 we summarize the results of a PCM-NP study[91] of the fluorescence of a model dye (perylene diimide, PDI) close to gold NPs of different shape and dimension. This example is here used to show the potential of the model not only to reproduce the expected enhancement but also to understand the underlying mechanisms. By comparing single-sphere and two-fused spheres NPs, a much more evident enhancement is seen for the latter case in the region of long distances and large radii, where neither the increase of the absorption nor that of the radiative process are at a maximum. This demonstrates that the enhancement is due to an optimal compromise between increased local field effects (larger radii) while keeping nonradiative losses at reasonable levels (longer distances). When we move from the PDI close to a single NP to the dye sandwiched between two NPs, the effect on $\Phi^{RB}$ is much more dramatic. The presence of two particles in the longitudinal orientation and positioned on the opposite end of the

dye increases the absorption and the radiative processes by orders of magnitude, whereas it "only" doubles the nonradiative process. Such nonlinear effects are automatically included in the PCM-NP calculation by the influence and mutual interaction of apparent charges on each NP. For this arrangement, the maximum increase is not for the region of long distances as in the previous case but for the region of short distances. In this region, the enhancement of $\Phi^{RB}$ is not due to relatively small nonradiative losses but to a large increase in the absorption and the radiative decay.

Turning now to QM/MM atomistic description, in ref. [83], the DIM model was extended to include not only the metal but also the functionalization layer, and proper rules to determine the metal atom polarizability parameters were developed. The properties of functionalized dimers of nanoparticles were calculated and experiments could be reproduced faithfully. More recently, the results of TERS experiments with sub-molecular resolution[28] have been also fully interpreted by applying the DIM model, without the need to perform any assumption on the localization degree of the electromagnetic field in the gap.[92] In the lower panel of Fig.3, the results of such an analysis are reported for a porphyrin molecule supported on a Au(111) slab. When a metal nanotip, modeled by a nanocrystal, is scanned over the molecule (see panel d of Fig.3), the (resonance) Raman scattering intensity for a given vibrational mode is calculated by DIM. The resulting intensity maps are reported for the out-of-plane motion of the outer and inner hydrogens: in both cases submolecular features are seen in agreement with experiments. Simulations of such features were performed before,[28] but the spatial distribution of the field was an input external parameter rather than part of the calculations itself.
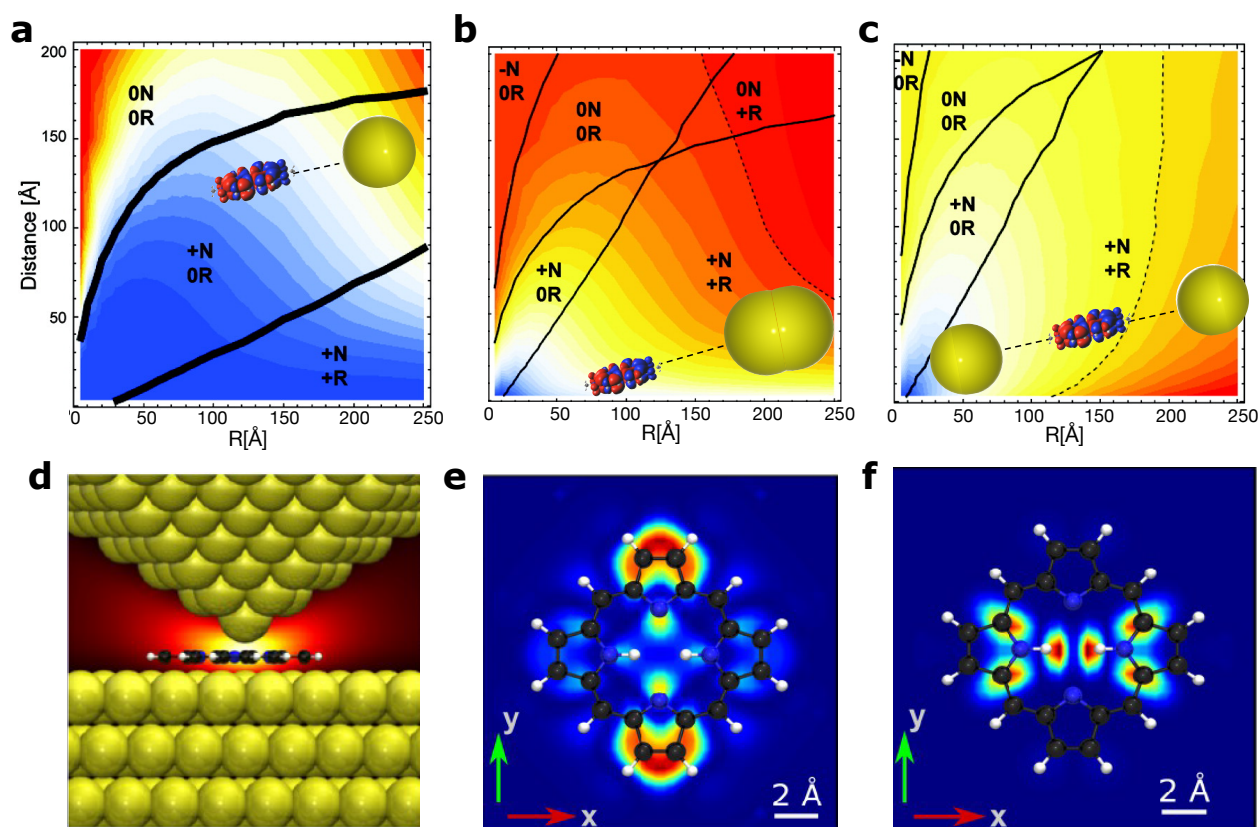


**Figure 2**. **Multiscale modeling of surface enhanced spectroscopy**. Upper panel: continuum PCM-NP modeling of Surface Enhanced Fluorescence of a model dye (PDI) close to gold nanoparticles.[91] Color scale plot of relative brightness $\Phi^{RB}$ with respect to dye-NP distance and NP radius (R). In all cases the PDI is placed with its long axis parallel to the NP long axis: a) a single sphere NP, b) a two-fused spheres NP, c) two coupled spherical NPs. N and R denote the nonradiative and radiative decay rates, respectively, and +, 0, and − indicate a larger, similar, and smaller metal-induced rate relative to the

isolated dye. The color scale is normalized with respect to the maximum $\Phi^{RB}$ value (red) for each system. For the single sphere NP, $\Phi^{RB}$ is always less than 1 whereas for the two other cases enhancements are possible (the combination of distance and radius values giving $\Phi^{RB} = 1$ are represented by a dotted line). All data refer to ZINDO calculations. Lower panel: atomistic DIM modeling of TERS of porphyrin.[92] d) Representation of the studied system, showing the gold surface, the porphyrin and the Au nanocrystal that simulates the nanotip. b) TERS intensity map for the 683 cm$^{-1}$ and c) 678 cm$^{-1}$ vibrational mode of porphyrin; these modes correspond to symmetric(asymmetric) out-of-plane motion of the outer(inner) hydrogens.[92] All data refer to TDDFT calculations. Upper panel adapted with permission from Ref. [91]; lower panel adapted with permission from Ref. [92], American Chemical Society.

**Photoresponsive proteins.** One of the most intriguing field of application for multiscale models is the investigation of the cascade of events that the absorption of sunlight can activate in proteins. The family of photoresponsive proteins is extremely large as they are involved in the most fundamental processes for life going from the photosynthesis used to produce the nutriment to live and grow to the sensory system used to interact with the outside world.[93,94] In all cases, the protein itself can be seen more as an embedding matrix than a real actor as the absorption of light is made possible by the presence of specific pigments, which are covalently or noncovalenty bound to the protein. These pigments, once in their excited states, activate the sequence of electronic and nuclear processes that, by crossing many different time and space scales, finally lead to the specific biological "function".

Here, in particular, we focus on the light harvesting (LH) function which is the initial light-induced step of photosynthesis. Through this process, the absorbed light is collected by the *antennae pigment-protein complexes* and efficiently funneled to the reaction center (the engine of the photosystem) where the energy is used to activate the first charge separation of the photosynthetic machinery. This apparatus is common to all photosynthetic organisms (plants, algae and bacteria) but the structure of the antennae and their pigment composition and configuration are very organism-dependent. [95] This shows that the LH antennae are the real "biological" component of the photosystem with their unique capacity to optimally adapt to the living condition of the organism. This adaptability is realized not only through the different chemical nature of the involved pigments and the structure of the protein matrix, but also with the exploitation of "collective" excitations going beyond the single pigment. In the antenna complex, in fact, (many) different pigments are packed in specific multichromophoric structures where the electronic interactions among the pigments generate new delocalized excitations (the excitons).[96,97] The latter can both enlarge the absorption capacity of the system and allow a much more efficient transfer of the absorbed energy to larger distances with respect to the analog system made of not localized excitations. The excitonic nature of LH complexes is made even more intriguing if we consider that the excitons "live" in conditions where fluctuations due to the dynamics of the protein and the disorder should act to destroy any electronic coherence. [98,99]

After many years of experimental and theoretical investigations, we now know that the LH complexes represent an optimized machinery to exploit the "natural" disorder for achieving the desired transfer efficiency through a delicate coupling between the electronic process and the network of vibrations within the pigments and across the protein.[100,101] In this long and difficult process towards a detailed understanding of the microscopic mechanisms of the LH function, the quantum mechanical modeling has clearly played a major role[86] even if, the large dimensions of the multichromophoric aggregates have forced to introduce approximated QM methods. Among them, the most effective one is the so called excitonic model where the Hamiltonian of the multichromophoric aggregate is built in terms of excitations localized in each pigment and their electronic couplings (see Box 3). This model has shown to be accurate for most of the LH complexes[97] but in some cases, the extremely dense packing of the pigments has introduced a further effect that this model cannot account for, namely an interpigment

charge-transfer (CT). Due to the mixing of these CT states with exciton states, the eigenstates of the antenna can be shifted, and the LH function can be changed. To account for CT effects, extensions of the excitonic model have been proposed. In particular, a possible strategy is that of introducing dimeric units to represent the CT states and using diabatic techniques to calculate the coupling of these states with the local excitation (LE) (see Box 3).

Moreover, it is now clear that a complete representation can only be achieved if the presence of the protein is explicitly included in the simulations. In fact, the different local environments felt by the pigments can differently change their excitations and consequently create or destroy possible resonances between them. The protein matrix can also affect the electronic couplings, either through a screening of the Coulomb interaction or by an enhancing of the transition properties of the single pigments (see Box 3). Moreover, the specific interactions of the protein residues and the embedded pigments can largely change the vibrational modes that couple to the electronic process even creating new ones of intermolecular nature. Finally, the protein, through its temperature-dependent fluctuations, introduces a disorder which perturbs the composition and the length of the excitons.

To account for all these effects, the multiscale approach combining QM and classical description represents an extremely effective strategy due to its unique characteristic of accounting for all the pieces of the problem, the pigments and their electronic interactions, the protein (with the external solvated membrane) and the dynamics of the whole system. Here, however, the multiscale model has to keep the atomistic and dynamic nature of the "environment" as well as it has to allow mutual polarization effects between the chromophoric aggregate and the environment. These requirements can be obtained using a polarizable embedding version of QM/MM approaches and integrating it with molecular dynamics simulations of the whole system.

To illustrate what insight this kind of investigation can achieve, we have selected a specific example, the major LH complex present in the photosystem of purple bacteria (commonly known as LH2).[102] The LH2 complex is an integral membrane antenna complex characterized by a cylindrical structure of C9 symmetry containing bacteriochlorophyll a (BChl) and carotenoid pigments (see panel a of Fig. 3).[103]
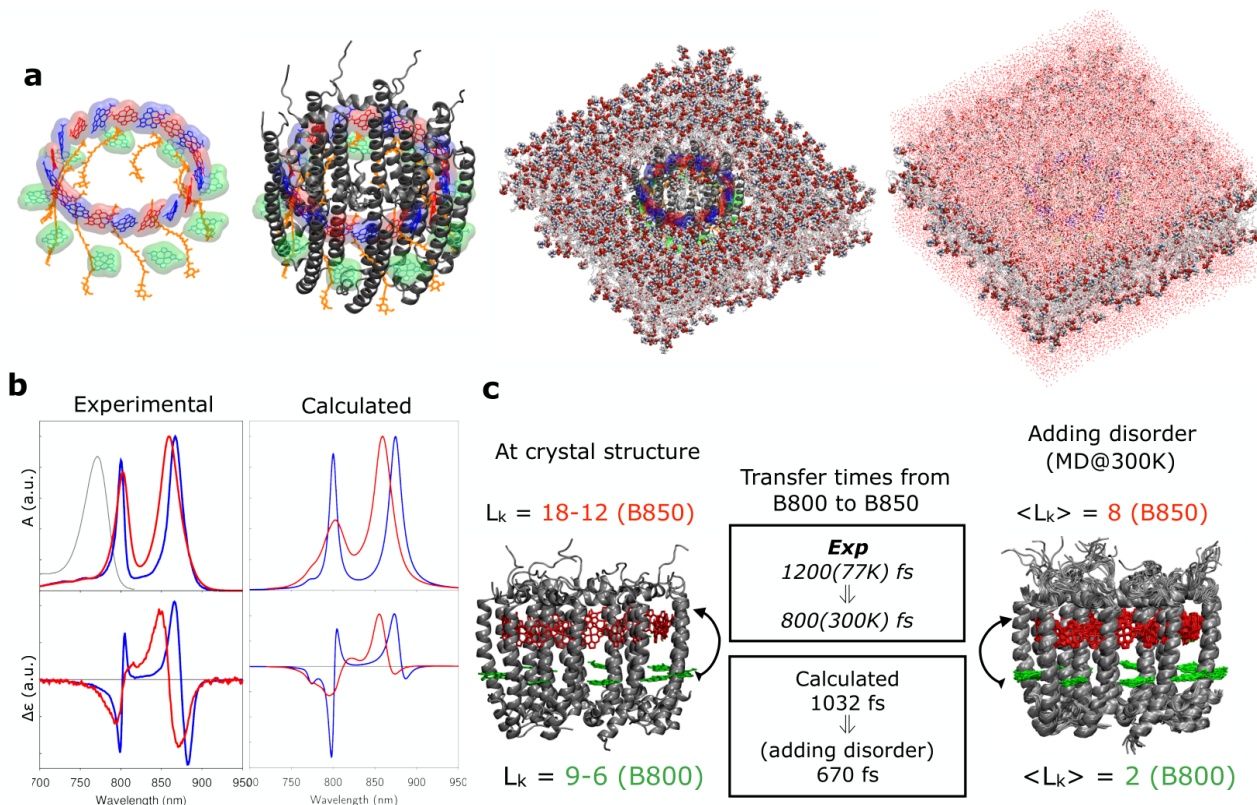
**Figure 3**. **The multiscale modeling of LH2**. a) Representation of the system with models of increasing realism, from left to right: the multichromophoric aggregate made of 27 bacteriochlorophyll *a* and 9 carotenoid pigments, the pigment-protein complex, the complex embedded in the membrane and the fully solvated system. b) Comparison between the experimental and the calculated absorption and CD spectra at very low (red, 77K in the experiments) and room temperature (blue).[104] c) Effect of temperature on the exciton lengths $L_k$ (see Box 3) and comparison between experimental[105] and calculated[106] inter ring (B800->B850) energy transfer times. All calculations refer to an excitonic TDDFT/MMPol model combined with classical molecular dynamics of the fully solvated system to account for temperature dependent fluctuations.

Among them, the pigments responsible for the LH function are the BChls which are arranged in two rings: one ring contains 9 BChls, whose molecular plane is perpendicular to the C9 axis whereas the other ring contains 18 BChls, whose molecular plane is perpendicular to the cylinder radius. The unique characteristic of LH2 with respect to other LH complexes is that it combines different excitonic subsystems which act together. In the ring containing the smaller number of BChl units, the electronic coupling is rather small and, as a result, the absorption band remains quite close to the one observed in the solvated BChl, namely at 800 nm (and the ring is called B800). On the contrary, in the second, much more densely packed, ring the couplings are stronger, and the resulting excitations are delocalized over a large number of pigments and CT states can also be possible.[107,108] Because of that, this ring is responsible for an absorption band largely red-shifted and appearing at 850 nm (and the ring is called B850). The excitonic nature of the system is also confirmed by the appearance of Circular Dichroism (CD) signals corresponding to the B800 and B850 excitations (see panel b of Fig.3). Because of its unique excitonic structure, three different mechanisms of transfer are expected, namely the one within the B800 ring, the other within the B850 ring and the third from the B800 to the B850 ring.[109-114]

To achieve a molecular-level analysis of all these aspects, a multiscale approach integrating MD simulations and QM/MM(pol) excitonic calculations of the whole solvated system have been performed and the results of these investigations can be summarized as follows: [104,106,115,116]

1) the excitonic characteristics of the system are profoundly affected by the environment through a combination of long-range electrostatic and shorter-range induction effects which define the energy ordering of the pigments and tune their electronic couplings;

2) at room temperature, the protein induced fluctuations in the relative orientation/distance of the densely packed pigments in the B850 ring lead to a decrease in the corresponding couplings: this is reflected in a blue-shift of both the absorption and CD bands (see panel b of Fig. 3) which the simulations show to be due to a localization of the excitons and correlate to the experimentally observed speed-up of the inter-ring transfer (see panel c of Fig.3);

3) the B850 ring involves BChl-BChl charge-transfer states which can mix with the excitons and this mixing is strongly affected by the environment both in terms of energy ordering and correlated disorder: this is reflected in broader spectra and a redistribution of the dipole strengths among the different excitons.

Combining all these findings, a better rational of the light-harvesting strategy of purple bacteria is possible. The highly symmetric structure of LH2 which suggests that the electronic states are delocalized over many pigments, and most of its lowest states are optically forbidden, is counterbalanced by a large sensitivity to even small perturbations such as those induced by minor fluctuations in the environment structural and electrostatic properties. This sensitivity is much more evident in the strongly coupled B850 ring which serves as final donor for the inter-complex transfer process towards the reaction center: here an efficient energy transfer can only be achieved if there is optimal energetic alignment between the emitting states of the donor complex and the absorbing states of the acceptor. Moreover, the absorption spectrum should be broad enough to allow for efficient light harvesting and energy funneling.[116]

**Towards composite systems.** Recently, the possibility to treat a QM molecule immersed in a MM layer in proximity of a continuum metal and surrounded by a continuum solvent has been implemented.[117,118] The implementation is fully self-consistent (i.e., the mutual polarizations of the quantum atomistic, the classical atomistic and the continuum regions are all accounted for). Its main field of application concerns complex biomolecules that contains chromophores, in the presence of plasmonic nanostructures. In fact, as commented above, the biomolecular matrix, while not directly excited by the light, is pivotal in determining the chromophore properties, and cannot be convincingly neglected. The approach that includes all these layers represented the state of the art of both solvation models and models for molecules close to metal nanostructures. Such multilayers models demonstrated their potential in different applications. In ref. [[117]], the model was shown to be able to reproduce the experimentally determined amplification of the fluorescence signal for a LH protein (PCP) in the presence of silver nanoparticles.[119] More interestingly, the calculations allowed to gain insights into the role of metal to modulate the various involved optical processes (absorption, emission, EET between the pigments), and led to formulate design rules for building hybrid bio-nano-systems. Successively, the multilayer model was used to investigate how a plasmonic nanostructure affects excitonic states of the LH2 complex.[120] Experimental studies have in fact shown that plasmonic nanoantennae can control excitation and emission of LH2 complexes.[121,122]

In particular, the goal was to verify whether it is possible to devise metal nanostructures able to drastically perturb the character of the LH2 exciton states, inducing localization effects of varying degrees. Based on the multiscale results, it was suggested that nanoplasmonic is indeed a viable strategy to achieve this goal.[120] The main point is to define the proper setup, namely tip-shaped gold nanoparticles displaying plasmon peaks in resonance with the absorption bands of LH2, either 800 or 850 nm, placed in correspondence to the resonant ring (Fig. 4, panel b). Using such an optimal setup, the plasmonic effect is not only seen in the enhancement of the absorption as already found for single chromophores. When inspecting the spatial properties of the exciton states, in fact, significant modifications appear as well because of the different local field effects acting on the different BChls due to their different distance and orientation with respect to the nanotip (NT). As a result, states that were dark and rather delocalized are now subject to a strong localization, with a consequent increase of the transition dipole moment. The practical implications of these modifications are indeed important. For example, if we simulate the effect of iradiating the system with light polarized along the NT axis, in energy ranges resonant with each tip, i.e., around 850 and 800 nm for NT-850 and NT-800, respectively, the results (reported in panel e of Fig. 4, "state superposition") show highly localized states on the tip side. At room temperature, such results could be completely overturned, should the disorder overcome the effect of the nanotip. In order to test this hypothesis, the effect of the static disorder has been modelled by adding a normally distributed noise on the site energies. The resulting average populations are reported in panel (e) of Fig. 4 ("Average population"). Clearly, the disorder does not significantly modify the picture obtained before, as the same spatial localization can be observed for both sets of excitations as before. Concerning specifically the B800 excitations, previously we have shown that, in the presence of static disorder, these excitations are very much localized already (see Fig. 3), owing to the small coupling between BChls. While this could seem to belittle the effect of the plasmon for the B800 excitations, it in fact suggests that the latter could act as a selector, allowing to selectively localize the excitation onto one particular BChl.
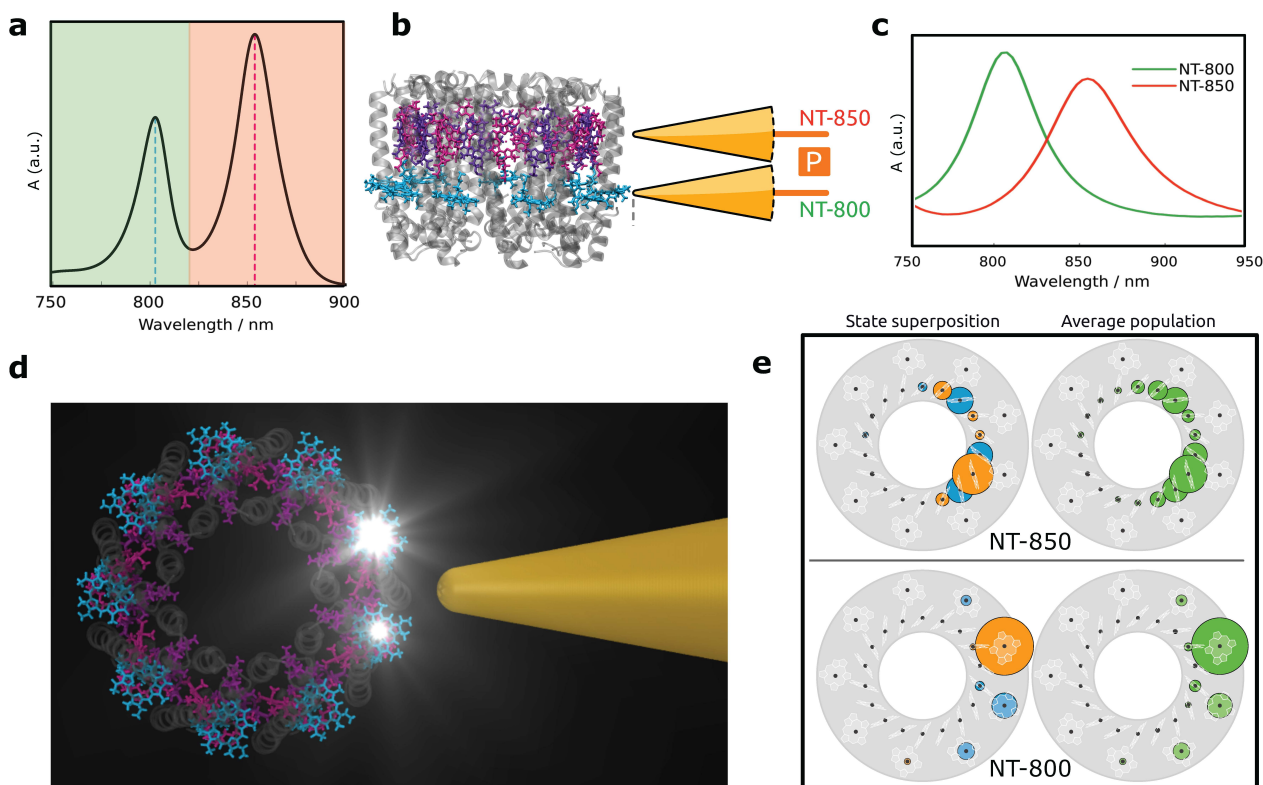
**Fig. 4**. **Plasmonic effects on excitons of LH2**. a) LH2 absorption spectrum with indication of the two wavelength regions of irradiation used for the two different nanotips. b) Arrangement of the two nanotips, NT-800 and NT-850, with respect to the LH2 complex; the polarization axis (labeled P) is perpendicular to the LH2 $C_9$ axis. c) Simulated extinction cross sections for NT-800 and NT-850. d) Pictorial representation of the effect of NT-800 on the excitons of the B800 ring. e) Simulation of the effect of light irradiation using NT-800 and light in the 750-820 nm range (bottom), or NT-850 and light in the 820-900 nm range (top): superposition of accessible states (left) and average population after including disorder (right). All simulations refer to an excitonic TDDFT/MMPol/PCM-NP model. Adapted with permission from REF.[120], Royal Society of Chemistry.

## Conclusion and outlook

The multiscale modelling is nowadays a well-established computational strategy to study structures, properties and processes of complex systems, especially of biological nature.[123-126] In more recent years, the QM-based version of multiscale models has been extended beyond the description of systems in their electronic ground state and applied to photoinduced processes. This extension has required to revise some theoretical and numerical aspects of the original formulations of the models as discussed here. Moreover, it has been a strong impulse to further widen their applicability to systems made of different coupled scales: the molecular one, where the photoactivation is localized on, the larger but still molecular embedding (such as a protein) and finally the nano (and meso) scale, for which the atomistic nature is not important anymore and coarser descriptions can be introduced which more effectively describe the response to electromagnetic fields.

What are the next steps in the development of these models? This is very difficult to say as the field is rapidly evolving and new challenges always appear.

There are however some directions that surely need to be deepened, or even newly explored, for the multiscale modeling to become a well-established and fully reliable approach for the prediction of the photoinduced activity in composite systems.

The first, fundamental, direction is that of the nuclear dynamics. Most of the applications presented in this review are based on a static picture, or alternatively, on the decoupling of the electronic process from the nuclear dynamics. It is instead more and more evident that the photoinduced activity in complex systems are largely determined by a significant coupling of the electronic process with nuclear motions inside the target and between the target and the environment. This clearly requires extending the multiscale approaches here discussed to explicit dynamics simulations. As matter of fact, Born-Oppenheimer (BO) MD techniques integrating a QM description (either at semiempirical or ab initio level) and mechanical and electrostatic MM embeddings are available since long time. Also nonadiabatic dynamics,[127] especially in their trajectory based formulations (such as surface hopping)[128] have been proposed in the literature and applied to (bio)molecular systems of increasing complexity.[14] Only recently, extensions of the MD techniques have been proposed also for polarizable embeddings but still within a BO approximation.[81,129]

The next step is to integrate the different classical descriptions (continuum and atomistic) into a nonadiabatic dynamics where mutual polarization effects between the target and the (multilayer)environment are kept. This is indeed an extremely challenging goal. First of all, the computational cost involved necessarily requires new numerical strategies in order to go beyond model systems and extremely short time-scales. In the last years, a large activity has been focused on improving the scaling of the QM calculations,[78,130-132] also by introducing novel semiempirical methods[133] including Density Functional tight binding.[134] However, also the classical models have to be reconsidered in terms of their scaling as, when coupled to fast QM methods, they can become the real bottleneck of the calculation. Some progress in this direction has been already achieved both within continuum models[135] and induced dipole formulations of the polarizable MM embedding.[136] However, the main difficulty here is from the theoretical point of view: the presence of a polarizable embedding in fact makes the environment effects state-specific and this introduces a specificity to nonadiabatic dynamics that has not been faced yet.

Still towards a much better scaling of the classical approaches for the dynamic simulation of systems of very large dimensions, it is worth recalling here the important progress seen in the last years in the accuracy and robustness of coarse grained (CG) force fields[137,138] that can now also include polarization effects. Examples of integration among different classical models (from atomistic to CG and continuum) have already been proposed in the literature[139,140] but this integration still needs to be enhanced to describe composite systems combing biomacromolecules, complex biological environments such as membranes and nonbiological nanostructures.

Another necessary direction to explore, is the introduction of possible "chemical" interactions between the target and the environment. This is particularly important in the case of (supra)molecular systems close to plasmonic nanoparticles. So far, in fact, the modeling of the metal has been based on descriptions that do not explicitly account for electrons. Photochemistry induced in the molecule by hot-carrier injections, a subject of great current interest, is therefore beyond the applicability of such models. Moreover, the process of exchanging electrons is pivotal to describe properly a venerable and still poorly characterized aspect of SERS (although not a dominant one), the chemical enhancement. The latter, beside a contribution coming from the ground state modification due to the molecule-metal interaction, is involving a resonant-Raman like effect due to a metal-molecule charge transfer state. A possible strategy is the introduction of "variable" boundaries between the target and the environment. This strategy has been already used in the QM/MM dynamical simulation of solvated molecules and liquids,[141] to allow the location and the contents of the QM subsystem to be updated when needed.

A third direction which needs to be explored is the one where the electromagnetic coupling between the (super)molecular system and the nanostructure can be large enough to take the system in the strong coupling regime, where the plasmonic and molecular excitations hybridize to give rise to mixed excitations called plexcitons.[142-144] The quantum nature of plasmons, in this framework, has been generally treated by extending the theory of quantization of electromagnetic field in free space

(Quantum ElectroDynamics, QED) [38] to the case where a plasmonic nanostructure (characterized as a continuous medium with dissipative dielectric constant) is present.[145,146] Multiscale models such as PCM-NP seem a good starting point to achieve a chemical description of molecules strong coupled to plasmonic nanostructure.

All these directions go towards an increased completeness of the simulations which is exactly what any good computational strategy should aim at. However, the philosophy beyond the multiscale description also wants to maintain a *focused* character, e.g. a hierarchical description of the different parts of the system. This strategy is, in some sense, opposite to what one could naturally think of, namely to extend the QM description to an increasingly larger part of the system. Nowadays, the latter strategy is indeed growingly possible thanks both to the new hardware infrastructures (e.g. through the graphical processing units and the many integrated core coprocessors) and the large progress in the computational efficiency of the softwares to take advantage of the former. In parallel, large and important progresses have been achieved in the field of quantum embedding methods.[147-149] In particular, DFT embedding approaches[150] such as the frozen density embedding have shown to be able to accurately describe photoinduced processes in complex systems combining mutichromophoric aggregates and biological matrices,[151] and were also used to describe plasmon-assisted photocatalysis.[152] Up to now, however, there are no doubts that the multiscale approach is still unbeatable in terms of efficiency and it will remain so for many years. We believe that the multiscale approach will stay even longer; its unique "control" of the different parts of the system through the selection of the optimal boundaries and the switch on/off for the interactions between them, is in fact an extremely effective tool. Through that, it is possible to achieve a so deep molecular-level understanding of the roles played by the different parts of the system that a fully QM description would hardly reach. The main challenge for the future of these models can therefore be summarized as follows: a preserved simplicity of interpretation combined with an enhanced realism.

**Box 1** The Apparent Surface Charge (ASC) formulation of continuum models

The basic formulation of continuum models requires the solution of a classical electrostatic problem (Poisson problem):

$$-\vec{\nabla} \cdot \left[ \varepsilon(\vec{r}) \vec{\nabla} V(\vec{r}) \right] = 4\pi \rho_M(\vec{r})$$

where $\rho_M$ is the solute charge distribution and $\varepsilon(r)$ is the general position-dependent permittivity. If we assume that the charge distribution $\rho_M$ is contained in a molecular cavity $C$ of proper shape and dimension built within a homogeneous and isotropic solvent, the following simplification can be used for $\varepsilon(r)$:

$$\varepsilon(\vec{r}) = \begin{cases} 1 & \vec{r} \in C \\ \varepsilon & \vec{r} \notin C \end{cases}$$

where $\varepsilon$ is the dielectric constant of the bulk medium.

Within this framework, and introducing the appropriate boundary conditions, the Poisson problem can be solved in terms of a potential $V$ which is the sum of the potential due to $\rho_M$ ($\phi_\rho$) plus the contribution due to a fictitious (or apparent) charge distribution on the surface of the cavity $C$, $\Gamma = \partial C$, namely:

$$V(\vec{r}) = \phi_\rho(\vec{r}) + V_\sigma(\vec{r})$$

$$V_\sigma(\vec{r}) = \int_\Gamma \frac{\sigma(\vec{s})}{|\vec{r} - \vec{s}|} d\vec{s}$$

Different alternative formulations of the apparent surface charge have been proposed in the literature which are known as different acronyms, the most popular ones being the family of the Polarizable Continuum Model (PCM)[21] and the Conductor Screening-like Solvation Model (COSMO).[20] Despites the differences in the theoretical model used, in all cases, an integral equation is introduced which can be recast as follows:

$$T\sigma = Rf_\rho$$

where $T$ and $R$ are integral operators which depend on the dielectric constant and the morphology of the cavity surface and $f_\rho$ is the electrostatic property due to $\rho_M$ calculated at the cavity surface (namely, an electric potential or the component of the electrostatic field perpendicular to the surface).

In spite of the remarkable simplification introduced by the use of the apparent surface charge (ASC) $\sigma$, the numerical resolution of the problem becomes challenging for a cavity of complex shape. To overcome this difficulty, a discrete representation of the surface $\Gamma$ in terms of a mesh made of N elements (often called *tesserae*), each characterized by a representative point $s_i$ and an area $a_i$, is generally introduce. This technique may be profitably linked to the boundary element method (BEM), a numerical technique widely used in physics and engineering to solve complex differential equations via numerical integration of integral equations. The discretization of $\Gamma$ automatically leads to a discretization of $\sigma$ in terms of point-like charges. Namely if we assume that on each surface element, $\sigma$ is practically constant, its effect can be simulated with a point charge $q_i = \sigma(\vec{s}_i)a_i$.

Within this framework, all integral operators become square matrices of dimension NxN, and the integral equation defining $\sigma$ is recast on a matrix equation for the point charges $q_i$.

The ASC model can also be applied to the continuum description of metal nanoparticles.[41] In this case, however, the dielectric becomes finite, with shape and dimension coinciding with those of the selected nanoparticle(s). The ASCs are now placed not on the surface of the molecular cavity but on the surface of the particle itself. Moreover, the ASCs acquire an imaginary part, i.e. they are complex numbers. The metal specimen, in fact behaves differently if interacting with static or oscillating fields. In the first case it has a conductor-like behaviour which, in the present context, corresponds to an infinite dielectric constant. In the second case, instead, the actual dielectric behaviour is recovered but the dielectric constant becomes a frequency dependent function, $\varepsilon(\omega)$, characterized by a real and an imaginary part, the latter connected to energy dissipation in the metal (see Box 4). Metal nanoparticles, in fact, absorb energy from the light and behave as a dissipative channel for excited state molecules placed in their vicinity.[153] In the literature on metal nanoparticles, ASCs approaches are most often called BEMs and they may also include apparent surface currents so to solve Maxwell equations and thus account for electromagnetic retardation effects.[154]

**Box 2** The Induced Dipole (ID) formulation of polarizable embedding within QM/MM

In their most common formulation, QM/MM methods introduces a direct interaction between the QM and the MM part only through electrostatics, using a fixed point-charge representation of the MM atoms. In the years, this electrostatic embedding formulation of QM/MM methods has been extended to include induction (or mutual polarization) effects between the two subsystems. One of the most popular way to effectively introduce this additional interaction is to use the induced dipole (ID) formulation. Within this framework, the MM atoms are described in terms of fixed point charges (or fixed multipolar distributions) and a polarizability (usually the isotropic static component). Because of that, each MM particle becomes a polarizable site which responds to an applied field generating an "atomic" induced dipole. The induce dipoles can be obtained through a matrix formaultion which is fully parallel to the one used to define the ASCs in Box 1:

$$\mathbf{R}\boldsymbol{\mu} = \mathbf{E}$$

where the vector $\mathbf{E}$ collects the electric field from the QM subsystem and the MM permanent charge distribution. The matrix $\mathbf{R}$ is determined uniquely by the position of the polarizable MM sites and the corresponding polarizabilities, namely:

$$\mathbf{R} = \begin{bmatrix} \alpha_1^{-1} & 0 & \cdots & 0 \\ 0 & \alpha_2^{-1} & \cdots & 0 \\ \vdots & \vdots & \ddots & \vdots \\ 0 & 0 & \cdots & \alpha_N^{-1} \end{bmatrix} + \begin{bmatrix} 0 & T_{12} & \cdots & T_{1N} \\ T_{21} & 0 & \cdots & T_{2N} \\ \vdots & \vdots & \ddots & \vdots \\ T_{N1} & T_{N2} & \cdots & 0 \end{bmatrix}$$

where $N$ is the number of polarizable sites and the dipole field tensor $T_{pq}$ is defined as

$$T_{pq} = \frac{\mathbf{1}}{r_{pq}^3} - \frac{3}{r_{pq}^5} \begin{bmatrix} x^2 & xy & xz \\ yx & y^2 & yz \\ zx & zy & z^2 \end{bmatrix}$$

Here $r_{pq}$ is the distance between site $p$ and $q$, and x, y and z are the Cartesian components of the vector connecting them.

Under certain conditions, two inducible dipoles at short distances can cause a "polarization catastrophe"; this effect can be imputed to the use of point polarizabilities instead of diffuse charge distributions. To avoid this problem, the 1–2 and 1–3 bonded polarization interactions can be turned off; alternatively, one can apply distance-dependent damping for interactions on short distances or use both procedures.[155] Several schemes for damping interactions between inducible dipoles at short distances have been proposed by Thole[156] by introducing distance-dependent screening functions to be used in the calculation of the dipole tensor $T_{pq}$. We also recall that the introduction of induced dipoles requires to re-parameterize the permanent charges with respect to the values used in an electrostatic embedding scheme.

Atomistic descriptions of metal nanoparticles (DIM and connected approaches)[82,84] closely follow this scheme as well. The most notable differences are that (i) the atomic polarizability becomes frequency dependent and a complex number, encoding in the imaginary part the dissipation of light by the metal (see box 4) and (ii) some versions of the approach include also the possibility that each atom develops a net charge. The value of the latter is determined by an equation similar to that for the dipole here above, with polarizabilities replaced by capacities and electric fields by electrostatic potentials.

---

**Box 3** The embedded exciton model

If we restrict our treatment to a two-level model for each site (ground and first excited state), and we allow only single-excitations , the electronic exciton Hamiltonian can be written as:

$$H_{ex} = \sum_n^N \varepsilon_n |n\rangle\langle n| + \sum_{n \neq m}^N V_{nm} |n\rangle\langle m|$$

$\varepsilon_n$ is the excitation energy of the *nth* site (often referred as *site energy*), whereas $V_{nm}$ is the *coupling* between excitations at site $n$ and $m$. $V_{nm}$ contains two main components, a Coulombic and an exchange term but the latter roughly decays exponentially with the intercromophoric distance[157] and, for separations higher than 1 nm, it can be safely neglected:

$$V_{mn} \approx V_{mn}^{Coul} = \int d\vec{r}\,' \int d\vec{r} \rho_m^T(\vec{r}\,') \frac{1}{\left|\vec{r} - \vec{r}\,'\right|} \rho_n^T(\vec{r})$$

$\rho^T_{m/n}$ are the transition densities for site $m/n$. Often $\rho^T_{m/n}$ are replaced by dipoles[158] but this approximation has to be used with care especially when the interchromophoric distances are of the same order of the molecular size of the chromophoric units.

The eigenvectors of the exciton Hamiltonian, often referred as *molecular excitons*, can be expressed as linear combinations of site excitations:

$$\left|K\right\rangle = \sum_{n=1}^{N} c_n^K \left|n\right\rangle$$

Because of the couplings $V_{mn}$, the excitons can be spread over the whole aggregate. To quantify this spread, it is useful to define the delocalization length of the K*th* exciton as:

$$1 \leq L_K = \left[\sum_n^N \left|c_n^K\right|^4\right]^{-1} \leq N$$

This quantity is referred as IPR (Inverse Participation Ratio). In the limit of localized states (that is, all $c_n^K = 0$ apart from one specific site with coefficient equal to 1), $L_K$ is one, while for fully delocalized states it reaches its maximum value, e.g. the number of units within the aggregate (N).

When the multichromophoric aggregate is embedded in an environment, site energies and couplings will be affected, through changes of the relative energies of ground and excited states of each site and the corresponding transition densities. Moreover, if the environment is allowed to respond to the excitation, being polarizable, an additional term will enter in the definition of the coupling: this term quantifies the interaction of each site with the polarization induced in the environment by the transition in another site. If an ASC continuum model is used to introduce a polarizable environment, such a term becomes: [159]

$$V_{mn}^{ASC} = \sum_k q_k^{ASC}\left(\rho_m^T\right) \cdot \int d\vec{r} \frac{\rho_n^T(\vec{r})}{\left|\vec{s}_k - \vec{r}\right|}$$

while for an ID formulation of a MM polarizable embedding we have[67]

$$V_{mn}^{MMpol} = -\sum_k \vec{\mu}_k^{ind}\left(\rho_m^T\right) \cdot \int d\vec{r} \frac{\rho_n^T(\vec{r})\left(\vec{r}_k - \vec{r}\right)}{\left|\vec{r}_k - \vec{r}\right|^3}$$

This additional term can be seen as a screening of the direct Coulomb interaction. Therefore, the neglect of polarization in the environment can give an overestimation of the coupling which can lead to a wrong description of the excitons and their delocalization.

The excitonic scheme can be extended to include charge-transfer (CT) states. To do that, one can: (i) define the chromophoric unit which describes the CT process (e.g. a dimer, a trimer etc.); (ii) calculate the excited states on such units; (iii) apply a diabatization approach to recover the "pure" (o diabatic) localized and CT states and the corresponding couplings. As a result, an extended exciton Hamiltonian is obtained:

$$H^{LE-CT} = H_{ex} + \sum_i^{N_{CT}} \varepsilon_i^{CT}\left|i\right\rangle\left\langle i\right| + \sum_n^N \sum_i^{N_{CT}} \left(V_{in}^{LE-CT}\left|i\right\rangle\left\langle n\right| + h.c.\right)$$

where the two additional terms correspond to the CT states and the couplings between locally excited (LE) and CT states, respectively. Also for this generalized approach, the effect of the environment can be determinant. In fact, the relative energy of LE and CT states will be strongly affected by the presence of a (polarizable) embedding. In the literature, different methods have been proposed to calculate couplings between LE and CT states,[160,161] but only recently these couplings have been combined with ab initio excitonic models.[115,162]

---

**Box 4** The optical response of metal nanoparticles

A key element of the "plasmonic" continuum model is the dielectric function used for metal nanoparticles. This function, together with the nanoparticle shape, size and embedding environment, determine the position and the width of the plasmonic resonance.[163] The physics of plasmonic resonances is grasped by the Drude dielectric function:

$$\varepsilon_D(\omega) = 1 - \frac{\Omega_p^2}{\omega^2 + i\omega\gamma} = 1 - \frac{\Omega_p^2}{\omega^2 + \gamma^2} + i\frac{\Omega_p^2\gamma}{\omega(\omega^2 + \gamma^2)}$$

where $\Omega_p$ is the plasma frequency of the metal (related to the electron density and effective electron mass) and $\gamma$ is a phenomenological damping rate. The imaginary part of $\varepsilon_D(\omega)$ is related to the absorption of light by the metal. With this dielectric function, the resonance frequency of the surface plasmon is size independent (up to nanoparticles radii $\sim 0.1 \cdot \lambda$ where electromagnetic retardation effects start to play a sizable role). For a spherical nanoparticle, the surface plasmon frequency is $\Omega_p/\sqrt{3}$. Drude dielectric function is in general not accurate enough to reproduce experimental results for metal such as gold and silver. In fact, it lacks the contribution of interband transitions. In such transitions, the electrons are promoted from a fully occupied band, e.g., that formed by the d orbitals of the metal, to a (partially) empty one, such as that formed by s and p orbitals. Experimentally measured dielectric function, tabulated as a function of frequency, are widely used as they naturally take into account all such effects.

In metal nanoparticles of dimensions smaller than 10 nm, the scattering of the electrons by the particle surface (absent in the metal bulk) starts to affect the damping of the plasmonic resonance. This is more relevant for the free electrons than for the interband transitions, and a widely used model dielectric function is: [164]

$$\varepsilon_K(\omega) = \varepsilon_{exp}(\omega) + \frac{\Omega_p^2}{\omega^2 + i\omega\gamma} - \frac{\Omega_p^2}{\omega^2 + i\omega\gamma'}$$

$$\gamma' = \gamma + A\frac{v_F}{R}$$

where $v_F$ is the Fermi velocity of the metal, and R is a geometrical parameter for the metal nanoparticle (the radius for a spherical NP). The constant $A$ is of the order of the unity and may in principle be calculated by geometric considerations. However, it can also be used as an external empirical parameter that account for the chemical nature of the metal surface (e.g. bare or chemically functionalized).

The use of a local dielectric constant for the metal (the polarization developed in a given point of the metal depends only on the total electric field in that point; in a non-local response the polarization depends on the electric fields in a region surrounding such point) is questionable for nanostructures with spatial gaps smaller than a few nm, for small NPs (< 3-5nm in diameter) and for molecules in close proximity of the nanoparticles. Various models are being developed to incorporate non-local effects, [165-167] but they have not been coupled with a first principle description of the molecule yet.

In atomistic models of the metal, the frequency dependence of the metal response is encoded in the atomic polarizability, $\alpha_i(\omega)$ and capacity, $C_i(\omega)$. The expressions that are used in the DIM are based on Lorentzian oscillators, namely: [168]

$$\alpha_i(\omega) = \alpha_{i,0}\left(\frac{\omega_{i,1}^2}{\omega_{i,1}^2 - \omega^2 - i\gamma_{i,1}\omega} + \frac{\omega_{i,2}^2}{\omega_{i,2}^2 - \omega^2 - i\gamma_{i,2}\omega}\right)$$

$$C_i(\omega) = C_{i,0}\frac{\omega_{i,1}^2}{\omega_{i,1}^2 - \omega^2 - i\gamma_{i,1}\omega}$$

where $\alpha_{i,0}$ is the static atomic polarizability (i.e., $\alpha_i(\omega) = \alpha_{i,0}$ by definition) and $C_{i,0}$ is the static atomic capacitance. The parameters $\omega_{i,1}$ and $\omega_{i,2}$ are the resonance frequencies and $\gamma_{i,1}$ and $\gamma_{i,2}$ the widths for the first and second oscillators, respectively. These are used as adjustable parameters to match higher level calculations. Recently, the coordination dependent DIM model has been introduced, where the parameters per each atom become dependent on its coordination environment (bulk, surface, edges and vertex atoms have therefore different frequency dependent polarizability), while capacity is not used. [83]

**Author contributions**

All authors contributed equally to the preparation of this manuscript.

**Competing interests**

The authors declare no competing interests.

References

1.      Ziegler, T. & Möglich, A. Photoreceptor engineering. *Front. Mol. Biosci.* **2,** 30 (2015).
2.      Xu, L., Mou, F., Gong, H., Luo, M. & Guan, J. Light-driven micro/nanomotors: from fundamentals to applications. *Chemical Society Reviews* **46,** 6905–6926 (2017).
3.      van Leeuwen, T., Lubbe, A. S., Štacko, P., Wezenberg, S. J. & Ben L Feringa. Dynamic control of function by light-driven molecular motors. *Nature Reviews Chemistry* **1,** 1–7 (2017).
4.      Wang, J., Xiong, Z., Zheng, J., Zhan, X. & Tang, J. Light-Driven Micro/Nanomotor for Promising Biomedical Tools: Principle, Challenge, and Prospect. *Acc. Chem. Res.* **51,** 1957–1965 (2018).
5.      Beljonne, D. & Cornil, J. *Multiscale Modelling of Organic and Hybrid Photovoltaics.* **352,** (Springer, 2014).
6.      Kilina, S., Kilin, D. & Tretiak, S. Light-Driven and Phonon-Assisted Dynamics in Organic and Semiconductor Nanostructures. *Chem. Rev.* **115,** 5929–5978 (2015).
7.      Alberi, K. *et al.* The 2019 materials by design roadmap. *J. Phys. D: Appl. Phys.* **52,** 013001–49 (2019).
8.      Warshel, A. & Levitt, M. Theoretical studies of enzymic reactions: dielectric, electrostatic and steric stabilization of the carbonium ion in the reaction of lysozyme. *Journal of Molecular Biology* **103,** 227–249 (1976).
9.      Rivail, J. L. & Rinaldi, D. A quantum chemical approach to dielectric solvent effects in molecular liquids. *Chemical Physics* **18,** 233–242 (1976).
10.     Miertuš, S., Scrocco, E. & Tomasi, J. Electrostatic interaction of a solute with a continuum. A direct utilizaion of AB initio molecular potentials for the prevision of solvent effects. *Chemical Physics* **55,** 117–129 (1981).
11.     Gao, J. Hybrid Quantum and Molecular Mechanical Simulations:  An Alternative Avenue to Solvent Effects in Organic Chemistry. *Acc. Chem. Res.* **29,** 298–305 (1996).
12.     Lin, H. & Truhlar, D. G. QM/MM: what have we learned, where are we, and where do we go from here? *Theoretical Chemistry Accounts* **117,** 185–199 (2006).
13.     Senn, H. M. & Thiel, W. QM/MM methods for biomolecular systems. *Angew. Chem. Int. Ed. Engl.* **48,** 1198–1229 (2009).
14.     Brunk, E. & Rothlisberger, U. Mixed Quantum Mechanical/Molecular Mechanical Molecular Dynamics Simulations of Biological Systems in Ground and Electronically Excited States. *Chem. Rev.* **115,** 6217–6263 (2015).
15.     Morzan, U. N. *et al.* Spectroscopy in Complex Environments from QM-MM Simulations. *Chem. Rev.* **118,** 4071–4113 (2018).
16.     Tomasi, J. & Persico, M. Molecular interactions in solution: an overview of methods based on continuous distributions of the solvent. *Chem. Rev.* **94,** 2027–2094 (1994).
17.     Cramer, C. J. & Truhlar, D. G. Implicit Solvation Models:  Equilibria, Structure, Spectra, and Dynamics. *Chem. Rev.* **99,** 2161–2200 (1999).
18.     Tomasi, J., Mennucci, B. & Cammi, R. Quantum Mechanical Continuum Solvation Models. *Chem. Rev.* **105,** 2999–3094 (2005).

19. Mennucci, B. Continuum solvation models: What else can we learn from them? *J. Phys. Chem. Lett.* **1,** 1666–1674 (2010).

20. Klamt, A. The COSMO and COSMO-RS solvation models. *WIREs Comput Mol Sci* **1,** 699–709 (2011).

21. Mennucci, B. Polarizable continuum model. *WIREs Comput Mol Sci* **2,** 386–404 (2012).

22. Onsager, L. Electric moments of molecules in liquids. *J. Am. Chem. Soc.* **58,** 1486–1493 (1936).

23. Cammi, R., Mennucci, B. & Tomasi, J. On the calculation of local field factors for microscopic static hyperpolarizabilities of molecules in solution with the aid of quantum-mechanical methods. *J. Phys. Chem. A* **102,** 870–875 (1998).

24. Aroca, R. F. Plasmon enhanced spectroscopy. *Physical Chemistry Chemical Physics* **15,** 5355–19 (2013).

25. Klingsporn, J. M., Sonntag, M. D., Seideman, T. & Van Duyne, R. P. Tip-Enhanced Raman Spectroscopy with Picosecond Pulses. *J. Phys. Chem. Lett.* **5,** 106–110 (2014).

26. Zrimsek, A. B. *et al.* Single-Molecule Chemistry with Surface- and Tip-Enhanced Raman Spectroscopy. *Chem. Rev.* **117,** 7583–7613 (2017).

27. Schlücker, S. Surface-Enhanced Raman Spectroscopy: Concepts and Chemical Applications. *Angew. Chem. Int. Ed.* **53,** 4756–4795 (2014).

28. Zhang, R. *et al.* Chemical mapping of a single molecule by plasmon-enhanced Raman scattering. *Nature* **498,** 82–86 (2013).

29. Kukura, P. Non-fluorescent schemes for single-molecule detection, imaging and spectroscopy. *Nature Photonics* **10,** 11–17 (2016).

30. Lakowicz, J. R. *et al.* Plasmon-controlled fluorescence: a new paradigm in fluorescence spectroscopy. *Analyst* **133,** 1308–39 (2008).

31. Dong, J., Zhang, Z., Zheng, H. & Sun, M. Recent Progress on Plasmon-Enhanced Fluorescence. *Nanophotonics* **4,** 1–19 (2015).

32. Mayer, K. M. & Hafner, J. H. Localized Surface Plasmon Resonance Sensors. *Chem. Rev.* **111,** 3828–3857 (2011).

33. Saha, K., Agasti, S. S., Kim, C., Li, X. & Rotello, V. M. Gold Nanoparticles in Chemical and Biological Sensing. *Chem. Rev.* **112,** 2739–2779 (2012).

34. Linic, S., Aslam, U., Boerigter, C. & Morabito, M. Photochemical transformations on plasmonic metal nanoparticles. *Nat Mater* **14,** 567–576 (2015).

35. Zhang, Y. *et al.* Surface-Plasmon-Driven Hot Electron Photochemistry. *Chem. Rev.* **118,** 2927–2954 (2018).

36. Zhan, C. *et al.* From plasmon-enhanced molecular spectroscopy to plasmon-mediated chemical reactions. *Nature Reviews Chemistry* **2,** 1–15 (2018).

37. Chikkaraddy, R. *et al.* Single-molecule strong coupling at room temperature in plasmonic nanocavities. *Nature* **535,** 127–130 (2016).

38. Ruggenthaler, M., Tancogne-Dejean, N., Flick, J., Appel, H. & Rubio, A. From a quantum-electrodynamical light–matter description to novel spectroscopies. *Nature Reviews Chemistry* **2,** 0118 (2018).

39. Sukharev, M. & Nitzan, A. Optics of exciton-plasmon nanomaterials. *Journal of Physics: Condensed Matter* **29,** 1–34 (2018).

40. Morton, S. M., Silverstein, D. W. & Jensen, L. Theoretical Studies of Plasmonics using Electronic Structure Methods. *Chem. Rev.* **111,** 3962–3994 (2011).

41. Corni, S. & Tomasi, J. Enhanced response properties of a chromophore physisorbed on a metal particle. *J. Chem. Phys.* **114,** 3739–13 (2001).

42. Garcia de Abajo, F. J. & Howie, A. Retarded field calculation of electron energy loss in inhomogeneous dielectrics. *Phys. Rev., B Condens. Matter* **65,** 4156–17 (2002).

43. Hohenester, U. & Trügler, A. MNPBEM – A Matlab toolbox for the simulation of plasmonic nanoparticles. *Computer Physics Communications* **183,** 370–381 (2012).

44. Delgado, A., Corni, S. & Goldoni, G. Modeling opto-electronic properties of a dye molecule in proximity of a semiconductor nanoparticle. *J. Chem. Phys.* **139,** 024105–12 (2013).

45. Neaton, J. B., Hybertsen, M. S. & Louie, S. G. Renormalization of Molecular Electronic Levels at Metal-Molecule Interfaces. *Phys. Rev. Lett.* **97,** 98–4 (2006).

46. Trautmann, S. *et al.* A classical description of subnanometer resolution by atomic features in metallic structures. *Nanoscale* **9,** 391–401 (2017).

47. Piatkowski, L., Accanto, N. & van Hulst, N. F. Ultrafast Meets Ultrasmall: Controlling Nanoantennas and Molecules. *ACS Photonics* **3,** 1401–1414 (2016).

48. Andrade, X. *et al.* Time-dependent density-functional theory in massively parallel computer architectures: the octopus project. *Journal of Physics: Condensed Matter* **24,** 233202–12 (2012).

49. Goings, J. J., Lestrange, P. J. & Li, X. Real-time time-dependent electronic structure theory. *WIREs Comput Mol Sci* **8,** e1341–19 (2017).

50. Coccia, E., Troiani, F. & Corni, S. Probing quantum coherence in ultrafast molecular processes: An ab initioapproach to open quantum systems. *J. Chem. Phys.* **148,** 204112–13 (2018).

51. Chen, H., McMahon, J. M., Ratner, M. A. & Schatz, G. C. Classical Electrodynamics Coupled to Quantum Mechanics for Calculation of Molecular Optical Properties: a RT-TDDFT/FDTD Approach. *J. Phys. Chem. C* **114,** 14384–14392 (2010).

52. Gao, Y. & Neuhauser, D. Communication: Dynamical embedding: Correct quantum response from coupling TDDFT for a small cluster with classical near-field electrodynamics for an extended region. *J. Chem. Phys.* **138,** 181105–5 (2013).

53. Sakko, A., Rossi, T. P., Enkovaara, J. & Nieminen, R. M. Atomistic approach for simulating plasmons in nanostructures. *Appl. Phys. A* **115,** 427–431 (2013).

54. Smith, H. T., Karam, T. E., Haber, L. H. & Lopata, K. Capturing Plasmon–Molecule Dynamics in Dye Monolayers on Metal Nanoparticles Using Classical Electrodynamics with Quantum Embedding. *J. Phys. Chem. C* **121,** 16932–16942 (2017).

55. Pipolo, S. & Corni, S. Real-Time Description of the Electronic Dynamics for a Molecule Close to a Plasmonic Nanoparticle. *J. Phys. Chem. C* **120,** 28774–28781 (2016).

56. Luque, F. J., Dehez, F., Chipot, C. & Orozco, M. Polarization effects in molecular interactions. *WIREs Comput Mol Sci* **1,** 844–854 (2011).

57. Rick, S. W., Stuart, S. J. & Berne, B. J. Dynamical fluctuating charge force fields: Application to liquid water. *J. Chem. Phys.* **101,** 6141–6156 (1994).

58. Hillier, I. H. Chemical reactivity studied by hybrid QM/MM methods. *Journal of Molecular Structure: THEOCHEM* **463,** 45–52 (1999).

59. Patel, S. & Brooks, C. L., III. Fluctuating charge force fields: recent developments and applications from small molecules to macromolecular biological systems. *Molecular Simulation* **32,** 231–249 (2006).

60. Lipparini, F. & Barone, V. Polarizable Force Fields and Polarizable Continuum Model: A Fluctuating Charges/PCM Approach. 1. Theory and Implementation. *J. Chem. Theory Comput.* **7,** 3711–3724 (2011).

61. Lipparini, F., Cappelli, C. & Barone, V. Linear Response Theory and Electronic Transition Energies for a Fully Polarizable QM/Classical Hamiltonian. *J. Chem. Theory Comput.* **8,** 4153–4165 (2012).

62. Boulanger, E. & Thiel, W. Solvent Boundary Potentials for Hybrid QM/MM Computations Using Classical Drude Oscillators: A Fully Polarizable Model. *J. Chem. Theory Comput.* **8,** 4527–4538 (2012).

63. Lemkul, J. A., Huang, J., Roux, B. & MacKerell, A. D., Jr. An Empirical Polarizable Force Field Based on the Classical Drude Oscillator Model: Development History and Recent Applications. *Chem. Rev.* **116,** 4983–5013 (2016).

64. Thompson, M. A. & Schenter, G. K. Excited States of the Bacteriochlorophyll b Dimer of Rhodopseudomonas viridis: A QM/MM Study of the Photosynthetic Reaction Center That Includes MM Polarization. *The Journal of Physical Chemistry* **99,** 6374–6386 (1995).

65. van Duijnen, P. T. & de Vries, A. H. Direct reaction field force field: A consistent way to connect and combine quantum-chemical and classical descriptions of molecules. *Int. J. Quantum Chem.* **60,** 1111–1132 (1996).

66. Illingworth, C. J. R., Parkes, K. E. B., Snell, C. R., Ferenczy, G. G. & Reynolds, C. A. Toward a Consistent Treatment of Polarization in Model QM/MM Calculations. *J. Phys. Chem. A* **112,** 12151–12156 (2008).

67. Curutchet, C. *et al.* Electronic Energy Transfer in Condensed Phase Studied by a Polarizable QM/MM Model. *J. Chem. Theory Comput.* **5,** 1838–1848 (2009).

68. Olsen, J. M. H. & Kongsted, J. *Chapter 3 - Molecular Properties through Polarizable Embedding. Advances in Quantum Chemistry* **61,** 107–143 (Elsevier Inc., 2011).

69. Jensen, L., van Duijnen, P. T. & Snijders, J. G. A discrete solvent reaction field model for calculating molecular linear response properties in solution. *J. Chem. Phys.* **119,** 3800–11 (2003).

70. Loco, D. *et al.* A QM/MM Approach Using the AMOEBA Polarizable Embedding: From Ground State Energies to Electronic Excitations. *J. Chem. Theory Comput.* **12,** 3654–3661 (2016).

71. van Duijnen, P. T., de Vries, A. H., Swart, M. & Grozema, F. Polarizabilities in the condensed phase and the local fields problem: A direct reaction field formulation. *J. Chem. Phys.* **117,** 8442–8453 (2002).

72. List, N. H., Jensen, H. J. X. R. A. & Kongsted, J. Local electric fields and molecular properties in heterogeneous environments through polarizable embedding. *Phys Chem Chem Phys* **18,** 1–11 (2016).

73. Chandrasekaran, S., Aghtar, M., Valleau, S., Aspuru-Guzik, A. & Kleinekathöfer, U. Influence of Force Fields and Quantum Chemistry Approach on Spectral Densities of BChl ain Solution and in FMO Proteins. *J. Phys. Chem. B* **119,** 9995–10004 (2015).

74. Andreussi, O., Prandi, I. G., Campetella, M., Prampolini, G. & Mennucci, B. Classical Force Fields Tailored for QM Applications: Is It Really a Feasible Strategy? *J. Chem. Theory Comput.* **13,** 4636–4648 (2017).

75. Cacelli, I. & Prampolini, G. Parametrization and Validation of Intramolecular Force Fields Derived from DFT Calculations. *J. Chem. Theory Comput.* **3,** 1803–1817 (2007).

76. Xu, P., Guidez, E. B., Bertoni, C. & Gordon, M. S. Perspective: Ab initio force field methods derived from quantum mechanics. *J. Chem. Phys.* **148,** 090901 (2018).

77. Gordon, M. S., Fedorov, D. G., Pruitt, S. R. & Slipchenko, L. V. Fragmentation Methods: A Route to Accurate Calculations on Large Systems. *Chem. Rev.* **112,** 632–672 (2012).

78. Gao, J. *et al.* Explicit Polarization: A Quantum Mechanical Framework for Developing Next Generation Force Fields. *Acc. Chem. Res.* **47,** 2837–2845 (2014).

79. Maurer, P., Laio, A., Hugosson, H. W., Colombo, M. C. & Rothlisberger, U. Automated Parametrization of Biomolecular Force Fields from Quantum Mechanics/Molecular Mechanics (QM/MM) Simulations through Force Matching. *J. Chem. Theory Comput.* **3,** 628–639 (2007).

80. Shen, L. & Yang, W. Molecular Dynamics Simulations with Quantum Mechanics/Molecular Mechanics and Adaptive Neural Networks. *J. Chem. Theory Comput.* **14,** 1442–1455 (2018).

81. Loco, D. *et al.* Hybrid QM/MM Molecular Dynamics with AMOEBA Polarizable Embedding. *J. Chem. Theory Comput.* **13,** 4025–4033 (2017).

82. Morton, S. M. & Jensen, L. A discrete interaction model/quantum mechanical method to describe the interaction of metal nanoparticles and molecular absorption. *J. Chem. Phys.* **135,** 134103–12 (2011).

83. Chen, X., Moore, J. E., Zekarias, M. & Jensen, L. Atomistic electrodynamics simulations of bare and ligand-coated nanoparticles in the quantum size regime. *Nature Communications* **6,** 1–8 (2015).

84. Li, X. *et al.* Optical Properties of Gold Nanoclusters Functionalized with a Small Organic Compound: Modeling by an Integrated Quantum-Classical Approach. *J. Chem. Theory Comput.* **12,** 3325–3339 (2016).

85. Walsh, T. R. & Knecht, M. R. Biointerface Structural Effects on the Properties and Applications of Bioinspired Peptide-Based Nanomaterials. *Chem. Rev.* **117,** 12641–12704 (2017).

86. Curutchet, C. & Mennucci, B. Quantum Chemical Studies of Light Harvesting. *Chem. Rev.* **117,** 294–343 (2017).

87. Mennucci, B. Modeling absorption and fluorescence solvatochromism with QM/Classical approaches. *Int. J. Quantum Chem.* **115,** 1202–1208 (2015).

88. List, N. H., Olsen, J. M. H. & Kongsted, J. Excited states in large molecular systems through polarizable embedding. *Phys Chem Chem Phys* **18,** 20234–20250 (2016).

89. Darby, B. L., Auguié, B., Meyer, M., Pantoja, A. E. & Le Ru, E. C. Modified optical absorption of molecules on metallic nanoparticles at sub-monolayer coverage. *Nature Photonics* **10,** 40–45 (2015).

90. Pelton, M. Modified spontaneous emission in nanophotonic structures. *Nature Photonics* **9,** 427–435 (2015).

91. Vukovic, S., Corni, S. & Mennucci, B. Fluorescence Enhancement of Chromophores Close to Metal Nanoparticles. Optimal Setup Revealed by the Polarizable Continuum Model. *J. Phys. Chem. C* **113,** 121–133 (2009).

92. Liu, P., Chulhai, D. V. & Jensen, L. Single-Molecule Imaging Using Atomistic Near-Field Tip-Enhanced Raman Spectroscopy. *ACS Nano* **11,** 5094–5102 (2017).

93. Kowalik, L. & Chen, J. K. Illuminating developmental biology through photochemistry. *Nature Chemical Biology* **13,** 587–598 (2017).

94. Kottke, T., Xie, A., Larsen, D. S. & Hoff, W. D. Photoreceptors Take Charge: Emerging Principles for Light Sensing. *Annu. Rev. Biophys.* (2018). doi:10.1146/annurev-biophys-070317-033047

95. Mirkovic, T. *et al.* Light Absorption and Energy Transfer in the Antenna Complexes of Photosynthetic Organisms. *Chem. Rev.* **117,** 249–293 (2017).

96. Saikin, S. K., Eisfeld, A., Valleau, S. & Aspuru-Guzik, A. Photonics meets excitonics: natural and artificial molecular aggregates. *Nanophotonics* **2,** 1–18 (2013).

97. Jang, S. J. & Mennucci, B. Delocalized excitons in natural light-harvesting complexes. *Rev. Mod. Phys.* **90,** 035003 (2018).

98. Collini, E. Spectroscopic signatures of quantum-coherent energy transfer. *Chem. Soc. Rev.* **42,** 4932–16 (2013).

99. Chenu, A. & Scholes, G. D. Coherence in Energy Transfer and Photosynthesis. *Annu. Rev. Phys. Chem.* **66,** 69–96 (2015).

100. Scholes, G. D. *et al.* Using coherence to enhance function in chemical and biophysical systems. *Nature* **543,** 647–656 (2017).

101. Jumper, C. C., Rafiq, S., Wang, S. & Scholes, G. D. ScienceDirect From coherent to vibronic light harvesting in photosynthesis. *Current Opinion in Chemical Biology* **47,** 39–46 (2018).

102.    Law, C. J. *et al.* The structure and function of bacterial light-harvesting complexes (Review). *Molecular Membrane Biology* **21,** 183–191 (2009).

103.    Cleary, L., Chen, H., Chuang, C., Silbey, R. J. & Cao, J. Optimal fold symmetry of LH2 rings on a photosynthetic membrane. *Proc. Natl. Acad. Sci. U.S.A.* **110,** 8537–8542 (2013).

104.    Cupellini, L. *et al.* An Ab Initio Description of the Excitonic Properties of LH2 and Their Temperature Dependence. *J. Phys. Chem. B* **120,** 11348–11359 (2016).

105.    Ma, Y.-Z., Cogdell, R. J. & Gillbro, T. Energy Transfer and Exciton Annihilation in the B800−850 Antenna Complex of the Photosynthetic Purple BacteriumRhodopseudomonas acidophila(Strain 10050). A Femtosecond Transient Absorption Study. *J. Phys. Chem. B* **101,** 1087–1095 (1997).

106.    Segatta, F. *et al.* A Quantum Chemical Interpretation of Two-Dimensional Electronic Spectroscopy of Light-Harvesting Complexes. *J. Am. Chem. Soc.* **139,** 7558–7567 (2017).

107.    Kunz, R. *et al.* Exciton Self Trapping in Photosynthetic Pigment–Protein Complexes Studied by Single-Molecule Spectroscopy. *J. Phys. Chem. B* **116,** 11017–11023 (2012).

108.    Ferretti, M. *et al.* Dark States in the Light-Harvesting complex 2 Revealed by Two-dimensional Electronic Spectroscopy. *Sci. Rep.* **6,** 20834 (2016).

109.    Herek, J. L. *et al.* B800-->B850 energy transfer mechanism in bacterial LH2 complexes investigated by B800 pigment exchange. *Biophysj* **78,** 2590–2596 (2000).

110.    Abramavicius, D., Valkunas, L. & van Grondelle, R. Exciton dynamics in ring-like photosynthetic light-harvesting complexes: a hopping model. *Physical Chemistry Chemical Physics* **6,** 3097–9 (2004).

111.    Novoderezhkin, V. I., Rutkauskas, D. & van Grondelle, R. Dynamics of the Emission Spectrum of a Single LH2 Complex: Interplay of Slow and Fast Nuclear Motions. *Biophys. J.* **90,** 2890–2902 (2006).

112.    Harel, E. & Engel, G. S. Quantum coherence spectroscopy reveals complex dynamics in bacterial light-harvesting complex 2 (LH2). *Proc. Natl. Acad. Sci. U.S.A.* **109,** 706–711 (2012).

113.    Smyth, C., Oblinsky, D. G. & Scholes, G. D. B800-B850 coherence correlates with energy transfer rates in the LH2 complex of photosynthetic purple bacteria. *Phys Chem Chem Phys* **17,** 30805–30816 (2015).

114.    van der Vegte, C. P., Prajapati, J. D., Kleinekathöfer, U., Knoester, J. & Jansen, T. L. C. Atomistic Modeling of Two-Dimensional Electronic Spectra and Excited-State Dynamics for a Light Harvesting 2 Complex. *J. Phys. Chem. B* **119,** 1302–1313 (2015).

115.    Nottoli, M. *et al.* The role of charge-transfer states in the spectral tuning of antenna complexes of purple bacteria. *Photosynth Res* **15,** 209–12 (2018).

116.    Cupellini, L. *et al.* Coupling to Charge Transfer States is the Key to Modulate the Optical Bands for Efficient Light Harvesting in Purple Bacteria. *J. Phys. Chem. Lett.* **9,** 6892–6899 (2018).

117.    Andreussi, O., Biancardi, A., Corni, S. & Mennucci, B. Plasmon-Controlled Light-Harvesting: Design Rules for Biohybrid Devices via Multiscale Modeling. *Nano Lett.* **13,** 4475–4484 (2013).

118.    Caprasecca, S., Guido, C. A. & Mennucci, B. Control of Coherences and Optical Responses of Pigment-Protein Complexes by Plasmonic Nanoantennae. *J. Phys. Chem. Lett.* **7,** 2189–2196 (2016).

119.    Mackowski, S. *et al.* Metal-Enhanced Fluorescence of Chlorophylls in Single Light-Harvesting Complexes. *Nano Lett.* **8,** 558–564 (2008).

120.    Caprasecca, S., Corni, S. & Mennucci, B. Shaping excitons in light-harvesting proteins through nanoplasmonics. *Chem. Sci.* **9,** 6219–6227 (2018).

121. Wientjes, E., Renger, J., Curto, A. G., Cogdell, R. & van Hulst, N. F. Strong antenna-enhanced fluorescence of a single light-harvesting complex shows photon antibunching. *Nature Communications* **5,** 4236 (2014).

122. Wientjes, E., Renger, J., Curto, A. G., Cogdell, R. & van Hulst, N. F. Nanoantenna enhanced emission of light-harvesting complex 2: the role of resonance, polarization, and radiative and non-radiative rates. *Physical Chemistry Chemical Physics* **16,** 24739–24746 (2014).

123. Warshel, A. Multiscale Modeling of Biological Functions: From Enzymes to Molecular Machines (Nobel Lecture). *Angew. Chem. Int. Ed.* **53,** 10020–10031 (2014).

124. Dans, P. D., Walther, J., Gómez, H. & Orozco, M. Multiscale simulation of DNA. *Current Opinion in Structural Biology* **37,** 29–45 (2016).

125. Chiricotto, M., Sterpone, F., Derreumaux, P. & Melchionna, S. Multiscale simulation of molecular processes in cellular environments. *Philosophical Transactions of the Royal Society A: Mathematical, Physical and Engineering Sciences* **374,** 20160225–13 (2016).

126. Amaro, R. E. & Mulholland, A. J. Multiscale methods in drug design bridge chemical and biological complexity in the search for cures. *Nature Reviews Chemistry* **2,** 0148 (2018).

127. Curchod, B. F. E. & Martínez, T. J. Ab Initio Nonadiabatic Quantum Molecular Dynamics. *Chem. Rev.* **118,** 3305–3336 (2018).

128. Tully, J. C. Perspective: Nonadiabatic dynamics theory. *J. Chem. Phys.* **137,** 22A301–7 (2012).

129. Wu, X., Clavaguéra, C., Lagardère, L., Piquemal, J.-P. & la Lande, de, A. AMOEBA Polarizable Force Field Parameters of the Heme Cofactor in Its Ferrous and Ferric Forms. *J. Chem. Theory Comput.* **14,** 2705–2720 (2018).

130. Akimov, A. V. & Prezhdo, O. V. Large-Scale Computations in Chemistry: A Bird's Eye View of a Vibrant Field. *Chem. Rev.* **115,** 5797–5890 (2015).

131. Cole, D. J. & Hine, N. D. M. Applications of large-scale density functional theory in biology. *Journal of Physics: Condensed Matter* **28,** 393001–32 (2016).

132. Giese, T. J. & York, D. M. Quantum mechanical force fields for condensed phase molecular simulations. *Journal of Physics: Condensed Matter* **29,** 1–14 (2017).

133. Thiel, W. Semiempirical quantum-chemical methods. *WIREs Comput Mol Sci* **4,** 145–157 (2013).

134. Elstner, M. & Seifert, G. Density functional tight binding. *Philosophical Transactions of the Royal Society A: Mathematical, Physical and Engineering Sciences* **372,** 20120483–20120483 (2014).

135. Lipparini, F. *et al.* Quantum Calculations in Solution for Large to Very Large Molecules: A New Linear Scaling QM/Continuum Approach. *J. Phys. Chem. Lett.* **5,** 953–958 (2014).

136. Lagardère, L. *et al.* Tinker-HP: a massively parallel molecular dynamics package for multiscale simulations of large complex systems with advanced point dipole polarizable force fields. *Chem. Sci.* **9,** 956–972 (2018).

137. Marrink, S. J. & Tieleman, D. P. Perspective on the Martini model. *Chem. Soc. Rev.* **42,** 6801–22 (2013).

138. Kmiecik, S. *et al.* Coarse-Grained Protein Models and Their Applications. *Chem. Rev.* **116,** 7898–7936 (2016).

139. Sokkar, P., Boulanger, E., Thiel, W. & Sanchez-Garcia, E. Hybrid Quantum Mechanics/Molecular Mechanics/Coarse Grained Modeling: A Triple-Resolution Approach for Biomolecular Systems. *J. Chem. Theory Comput.* **11,** 1809–1818 (2015).

140. Ricci, C. G., Li, B., Cheng, L.-T., Dzubiella, J. & McCammon, J. A. 'Martinizing' the Variational Implicit Solvent Method (VISM): Solvation Free Energy for Coarse-Grained Proteins. *J. Phys. Chem. B* **121,** 6538–6548 (2017).

141. Duster, A. W., Wang, C.-H., Garza, C. M., Miller, D. E. & Lin, H. Adaptive quantum/molecular mechanics: what have we learned, where are we, and where do we go from here? *WIREs Comput Mol Sci* **103,** e1310–21 (2017).

142. Sugawara, Y., Kelf, T. A., Baumberg, J. J., Abdelsalam, M. E. & Bartlett, P. N. Strong Coupling between Localized Plasmons and Organic Excitons in Metal Nanovoids. *Phys. Rev. Lett.* **97,** 266808–4 (2006).

143. Fofang, N. T. *et al.* Plexcitonic Nanoparticles: Plasmon–Exciton Coupling in Nanoshell–J-Aggregate Complexes. *Nano Lett.* **8,** 3481–3487 (2008).

144. Beane, G., Brown, B. S., Johns, P., Devkota, T. & Hartland, G. V. Strong Exciton–Plasmon Coupling in Silver Nanowire Nanocavities. *J. Phys. Chem. Lett.* **9,** 1676–1681 (2018).

145. Jacob, Z. & Shalaev, V. M. Plasmonics goes quantum. *Science* **334,** 463–464 (2011).

146. Tame, M. S. *et al.* Quantum plasmonics. *Nature Physics* **9,** 329–340 (2013).

147. Libisch, F., Huang, C. & Carter, E. A. Embedded Correlated Wavefunction Schemes: Theory and Applications. *Acc. Chem. Res.* **47,** 2768–2775 (2014).

148. Wesolowski, T. A., Shedge, S. & Zhou, X. Frozen-Density Embedding Strategy for Multilevel Simulations of Electronic Structure. *Chem. Rev.* **115,** 5891–5928 (2015).

149. Sun, Q. & Chan, G. K.-L. Quantum Embedding Theories. *Acc. Chem. Res.* **49,** 2705–2712 (2016).

150. Jacob, C. R. & Neugebauer, J. Subsystem density-functional theory. *WIREs Comput Mol Sci* **4,** 325–362 (2014).

151. König, C. & Neugebauer, J. Quantum Chemical Description of Absorption Properties and Excited-State Processes in Photosynthetic Systems. *ChemPhysChem* **13,** 386–425 (2011).

152. Spata, V. A. & Carter, E. A. Mechanistic Insights into Photocatalyzed Hydrogen Desorption from Palladium Surfaces Assisted by Localized Surface Plasmon Resonances. *ACS Nano* **12,** 3512–3522 (2018).

153. Andreussi, O., Corni, S., Mennucci, B. & Tomasi, J. Radiative and nonradiative decay rates of a molecule close to a metal particle of complex shape. *J. Chem. Phys.* **121,** 10190–13 (2004).

154. Myroshnychenko, V. *et al.* Modelling the optical response of gold nanoparticles. *Chem. Soc. Rev.* **37,** 1792–1805 (2008).

155. Van Duijnen, P. T. & Swart, M. Molecular and atomic polarizabilities: Thole's model revisited. *J. Phys. Chem. A* **102,** 2399–2407 (1998).

156. Thole, B. T. Molecular polarizabilities calculated with a modified dipole interaction. *Chemical Physics* **59,** 341–350 (1981).

157. Dexter, D. L. A theory of sensitized luminescence in solids. *J. Chem. Phys.* **21,** 836 (1953).

158. Főrster, T. 10th Spiers Memorial Lecture. Transfer mechanisms of electronic excitation. *Discuss. Faraday Soc.* **27,** 7–17 (1959).

159. Iozzi, M. F., Mennucci, B., Tomasi, J. & Cammi, R. Excitation energy transfer (EET) between molecules in condensed matter: A novel application of the polarizable continuum model (PCM). *J. Chem. Phys.* **120,** 7029–12 (2004).

160. Hsu, C. P., You, Z. Q. & Chen, H. C. Characterization of the Short-Range Couplings in Excitation Energy Transfer. *J. Phys. Chem. C* **112,** 1204–1212 (2008).

161. Difley, S. & Van Voorhis, T. Exciton/Charge-Transfer Electronic Couplings in Organic Semiconductors. *J. Chem. Theory Comput.* **7,** 594–601 (2011).

162. Li, X., Parrish, R. M., Liu, F., Kokkila Schumacher, S. I. L. & Martínez, T. J. An Ab Initio Exciton Model Including Charge-Transfer Excited States. *J. Chem. Theory Comput.* **13,** 3493–3504 (2017).

163. Yu, R., n, L. M. L.-M. X. & de Abajo, F. J. G. X. A. Universal analytical modeling of plasmonic nanoparticles. *Chemical Society Reviews* **46,** 6710–6724 (2017).

164. Kreibig, U. & Fragstein, von, C. The limitation of electron mean free path in small silver particles. *Zeitschrift für Physik* **224,** 307–323 (1969).

165. Ciracì, C. *et al.* Probing the ultimate limits of plasmonic enhancement. *Science* **337,** 1072–1074 (2012).

166. Raza, S., Wubs, M., ndergaard, T. S. O., Bozhevolnyi, S. I. & Mortensen, N. A. A generalized non-local optical response theory for plasmonic nanostructures. *Nature Communications* **5,** 1–7 (2014).

167. Ciracì, C. & Sala, Della, F. Quantum hydrodynamic theory for plasmonics: Impact of the electron density tail. *Phys. Rev. B* **93,** 263–14 (2016).

168. Jensen, L. L. & Jensen, L. Atomistic Electrodynamics Model for Optical Properties of Silver Nanoclusters. *J. Phys. Chem. C* **113,** 15182–15190 (2009).